Geochemistry Geophysics Geosystems G3
AN ELECTRONIC JOURNAL OF THE EARTH SCIENCES
Published by AGU and the Geochemical Society

Article
Volume 8, Number 6
23 June 2007
Q06022, doi:10.1029/2006GC001559
ISSN: 1525-2027

Evolution of the Southwest Indian Ridge from 55°45′E to 62°E: Changes in plate-boundary geometry since 26 Ma

A. Graham Baines
Department of Geology and Geophysics, University of Wyoming, Laramie, Wyoming 82071, USA

Now at School of Earth and Environmental Sciences, Adelaide University, Adelaide, SA 5005, Australia (graham.baines@adelaide.edu.au)

Michael J. Cheadle
Department of Geology and Geophysics, University of Wyoming, Laramie, Wyoming 82071, USA

Henry J. B. Dick
Woods Hole Oceanographic Institution, Woods Hole Road, Woods Hole, Massachusetts 02543, USA

Allegra Hosford Scheirer
U.S. Geological Survey, 345 Middlefield Road, Menlo Park, California 94025, USA

Barbara E. John
Department of Geology and Geophysics, University of Wyoming, Laramie, Wyoming 82071, USA

Nick J. Kusznir
Department of Earth Sciences, University of Liverpool, Liverpool L69 3BX, UK

Takeshi Matsumoto
Department of Physics and Earth Sciences, University of the Ryukyus, 1 Senbaru, Nishihara-cho, Okinawa, 903-0213 Japan

[1] From 55°45′E to 58°45′E and from 60°30′E to 62°00′E, the ultraslow-spreading Southwest Indian Ridge (SWIR) consists of magmatic spreading segments separated by oblique amagmatic spreading segments, transform faults, and nontransform discontinuities. Off-axis magnetic and multibeam bathymetric data permit investigation of the evolution of this part of the SWIR. Individual magmatic segments show varying magnitudes and directions of asymmetric spreading, which requires that the shape of the plate boundary has changed significantly over time. In particular, since 26 Ma the Atlantis II transform fault grew by 90 km to reach 199 km, while a 45-km-long transform fault at 56°30′E shrank to become an 11 km offset nontransform discontinuity. Conversely, an oblique amagmatic segment at the center of a first-order spreading segment shows little change in orientation with time. These changes are consistent with the clockwise rotation of two ~450-km-wide first-order spreading segments between the Gallieni and Melville transform faults (52–60°E) to become more orthogonal to spreading. We suggest that suborthogonal first-order spreading segments reflect a stable configuration for mid-ocean ridges that maximizes upwelling rates in the asthenospheric mantle and results in a hotter and weaker ridge-axis that can more easily accommodate seafloor spreading.

Components: 16,054 words, 12 figures, 3 tables.

Keywords: Southwest Indian Ridge; Atlantis II fracture zone; asymmetric spreading; ridge segmentation.

Index Terms: 3035 Marine Geology and Geophysics: Midocean ridge processes; 3005 Marine Geology and Geophysics: Marine magnetics and paleomagnetics (1550); 3039 Marine Geology and Geophysics: Oceanic transform and fracture zone processes.

Received 17 December 2006; **Revised** 14 March 2007; **Accepted** 26 March 2007; **Published** 23 June 2007.

Baines, A. G., M. J. Cheadle, H. J. B. Dick, A. H. Scheirer, B. E. John, N. J. Kusznir, and T. Matsumoto (2007), Evolution of the Southwest Indian Ridge from 55°45′E to 62°E: Changes in plate-boundary geometry since 26 Ma, *Geochem. Geophys. Geosyst.*, *8*, Q06022, doi:10.1029/2006GC001559.

1. Introduction

[2] Our knowledge of tectonic and magmatic processes occurring at ultraslow-spreading ridges (full-spreading rate <20 km/Myr) has been significantly increased by recent studies that have focused on the axial structure of both the SWIR [*Dick et al.*, 2003; *Grindlay et al.*, 1998; *Mendel et al.*, 1997, 2003; *Cannat et al.*, 1999, 2003; *Sauter et al.*, 2001, 2004] and the Gakkel Ridge [*Dick et al.*, 2003; *Cochran et al.*, 2003; *Michael et al.*, 2003]. In particular, amagmatic spreading segments have been identified on these ridges and it has been argued that these represent a previously unrecognized class of plate boundary structure [*Dick et al.*, 2003]. Unlike accretionary magmatic segments, which form suborthogonal to the plate spreading direction, amagmatic segments form at any orientation relative to plate spreading and may replace both transform faults and accretionary magmatic segments. Amagmatic accretionary segments form at effective full-spreading rates <12 km/Myr [*Dick et al.*, 2003], where the effective full-spreading rate is defined as the component of the full-spreading rate perpendicular to the trend of the spreading segment, and commonly link with magmatic segments to form a plate boundary geometry characteristic of ultraslow-spreading rates.

[3] The regional trend of the SWIR between 52°E and 61°E is oblique to the spreading direction and, over a relatively short distance, accretionary magmatic segments are separated not only by oblique amagmatic segments, but also by transform faults and nontransform discontinuities (Figures 1 and 2). This section of the SWIR formed by northeastward propagation of the ridge-ridge-ridge Rodriguez Triple Junction between oceanic lithosphere created at the Central Indian (CIR) and Southeast Indian Ridges (SEIR) [*Patriat and Courtillot*, 1984; *Patriat and Segoufin*, 1988] (Figure 1), so the geometry and segmentation of the eastern SWIR cannot be attributed to the preexisting structure of a rifted continent as has been inferred for the Mid-Atlantic Ridge (MAR) [e.g., *Klitgord and Schouten*, 1986]. Also, unlike the East Pacific Rise where much of the lithosphere has been subducted [e.g., *Atwater*, 1989], the entire history of spreading along the eastern SWIR is available for study. These properties make the eastern SWIR, an excellent locality to study ridge segmentation and the genesis and evolution of oblique amagmatic spreading segments, nontransform discontinuities and transform faults.

[4] Segmentation at mid-ocean ridges has been discussed by many authors [e.g., *Batiza*, 1996; *Macdonald et al.*, 1988] who have defined a hierarchy of segmentation from 10^3 km down to 10^1 km. The largest (or first-order) scale of segmentation is usually defined by major transform faults spaced 10^2–10^3 km apart [*Macdonald et al.*, 1988]. These first-order segments or "tectonic corridors" are not defined solely by transform offsets but also by changes in basalt chemistry [*Sinton et al.*, 1991], off-axis subsidence, axial depth and the rate at which the geoid decreases off-axis [*Kane and Hayes*, 1992; *Hayes and Kane*, 1994]. The ridge-axis within these first-order segments is divided, on the scale of 10^1–10^2 km, into second and third order segments, defined by smaller offsets of the ridge, variations in axial depth and/or mantle Bouguer anomalies (MBA). This scale of segmentation may be related to more local shallow processes such as three-dimensional buoyant mantle flow, melt generation and/or melt migration [*Whitehead et al.*, 1984; *Macdonald et al.*, 1988; *Dick*, 1989; *Magde and Sparks*, 1997]. The eastern SWIR shows first-order segmentation on the order of 450 km defined by the Gallieni, Atlantis II

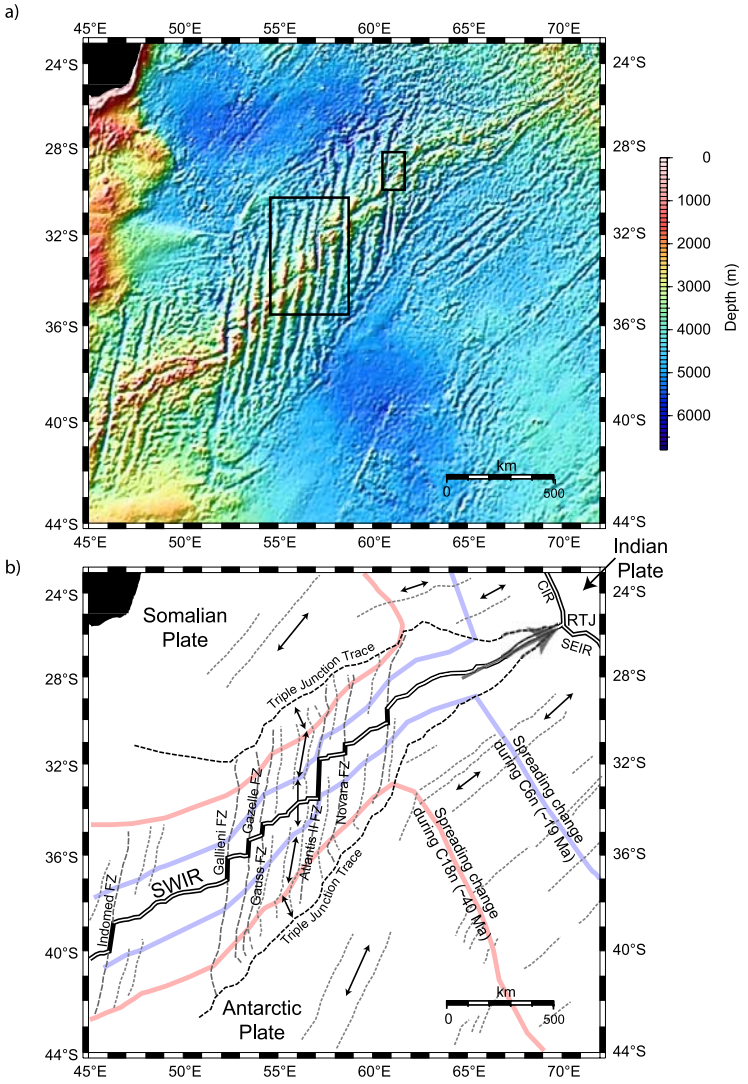

Figure 1. (a) The bathymetry of the SWIR from satellite gravity data [*Smith and Sandwell*, 1997]. Black boxes delimit the areas of Figures 2 and 5. (b) Interpretation of Figure 1a showing triple junction traces (black dashed lines), the current ridge axis (double black line), transform faults (thick black lines), and the trends of fracture zones (gray dashed lines). We show isochrons C6n (~19 Ma) and C18n (~40 Ma) after *Müller et al.* [1997]; these anomalies are relatively easy to map regionally and formed at approximately the time of major changes in plate spreading direction. We also show the apparent spreading directions determined from fracture zone orientation (double headed arrows). RTJ, Rodriguez Triple Junction; SWIR, Southwest Indian Ridge; SEIR, Southeast Indian Ridge; CIR, Central Indian Ridge.

and Melville transform faults; and second-order segmentation on the order of 70 km defined by oblique spreading segments, nontransform discontinuities and shorter transform faults (the Gazelle, Gauss and Novara transform faults) (Figure 1).

[5] The bathymetry of the SWIR and surrounding regions provides an important tool to understand the history of plate spreading in this region. Focal mechanisms determined for oceanic transform faults have long been recognized as predominantly strike-slip [e.g., *Sykes*, 1967], suggesting transform faults form parallel to the direction of plate-spreading. Consequently the orientation of fracture zones reflects the direction of plate spreading at the time the fracture zone formed. Two changes in plate spreading direction are recognized from the orientation of the fracture zones in this region. *Dick et al.* [1991] suggested that a change in the trace of the Atlantis II transform fault (Figure 2) indicates a counter clockwise rotation in plate-spreading direction 17–20 Ma. Bathymetric and magnetic data from the Novara Fracture Zone [*Hosford et al.*,

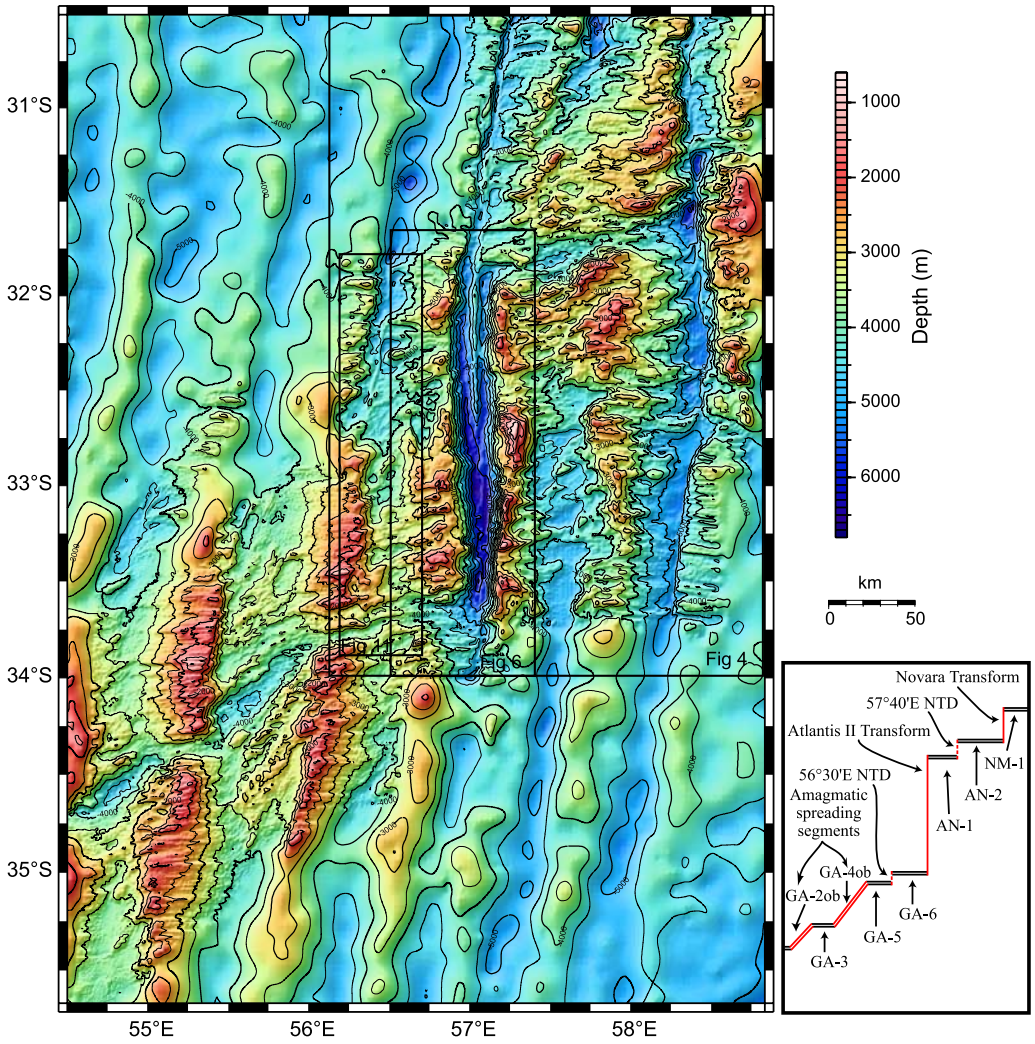

Figure 2. The SWIR from 54°45′E to 58°45′E. Combined multibeam bathymetry and satellite-derived bathymetry. Multibeam data are from *Mendel et al.* [1997], *Hosford et al.* [2003], and *Baines et al.* [2003], while satellite-derived bathymetry data are from *Smith and Sandwell* [1997]. Black boxes delimit the areas of Figures 4, 6, and 11. Inset shows the nomenclature of the ridge segments and offsets shown in the bathymetry.

2003] reveal that this was a 10° counterclockwise rotation in plate-spreading from 10°E before C6n to 0°E after C6n (∼19.2 Ma using the timescale of *Lourens et al.* [2004]) (Figure 1b). Further from the ridge axis (>40 Ma), the expression of the fracture zones becomes more chaotic (Figure 1a). Here the predominant orientation of the fracture zones is NNW-SSE (∼335°E) suggesting an ∼35° clockwise rotation in spreading direction ∼40 Ma. This change in spreading direction is also contemporaneous with a change in the orientation of fracture zones that formed at the SEIR suggesting a major change in plate kinematics at this time (Figure 1b). If we assume that the regional ($>10^2$–10^3 km) trend of the ridge axis has remained approximately constant through time and that magmatic spreading segments will rotate to become subperpendicular to spreading; then changes in plate spreading direction will lead to significant changes in the total length of spreading-parallel ridge offsets (Figure 3). The rotations in plate spreading direction identified at 40 Ma and 19.2 Ma would increase and decrease the length of spreading-parallel ridge offsets, respectively, and thus provide a driving force for changes in ridge geometry. In the following, we will consider the role that these rotations have played on the development of segmentation and spreading-parallel ridge offsets at the SWIR.

[6] From 54°45′E to 58°45′E on the SWIR, several studies have collected a large quantity of off-axis

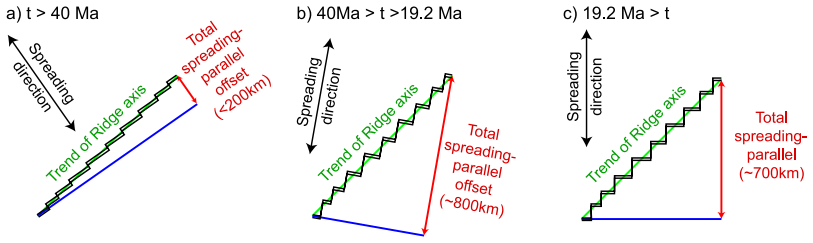

Figure 3. Cartoons of the possible effect of rotations in plate-spreading direction on ridge geometry at the SWIR between 52°E and 61°E. (a) Assuming a 045°N regional orientation of the ridge, an initial NNW-SSE spreading direction means that the ridge was initially suborthogonal to the spreading direction. (b) Following a rotation in spreading direction ~40 Ma to 010°N, the ridge was became oblique to spreading. (c) The 10° counterclockwise rotation in spreading direction ~19.2 Ma slightly reduced the SWIR's obliquity to the spreading direction. Red arrows show how the total spreading-parallel offset of the ridge varies in response to the changes in spreading direction.

multibeam bathymetric and sea-surface magnetic data [*Dick et al.*, 1991; *Hosford et al.*, 2003; *Patriat et al.*, 1996, 1997]. New data collected during the YK01-14 cruise of the R/V *Yokosuka* (Figure 4a) [*Matsumoto et al.*, 2002] completes off-axis coverage between data collected during earlier JAMSTEC cruises [*Hosford et al.*, 2003] and the Gallieni cruise (R/V *L'Atalante*, 1995) [*Patriat et al.*, 1996; *Mendel et al.*, 2003; *Sauter et al.*, 2004]. Together these studies provide >130,000 km^2 of continuous multibeam bathymetric coverage and extend for >400 km along the SWIR and 10–30 Ma away from it (Figure 2 and Figure 4). Consequently these data provide an ideal opportunity to compare and contrast the evolution of oblique amagmatic spreading segments, nontransform discontinuities and transform faults over a relatively narrow region of the SWIR where plate spreading rates, mantle composition, mantle potential temperature and, therefore the magma budgets to the adjacent segments are similar [e.g., *Cannat et al.*, 1999].

[7] During the KR00-06 R/V *Karei*/DSV *Kaiko* cruise to Atlantis Bank [*Kinoshita et al.*, 2001] bathymetric and magnetic data were also collected east of the Melville transform fault from 61°E to 62°E and to >15 Ma on both ridge flanks (Figure 5). We include analyses of these data here and use them together with the data from 54°45′E to 58°45′E to make broad inferences about the evolution of ridge offsets at the SWIR on the basis of plate-spreading rates determined from magnetic data.

2. Regional Setting

[8] The eastern SWIR (46°E–70°E) is an ultra-slow-spreading ridge with a full-spreading rate of ~14 km/Myr north-south that varies little over its length (Table 1) [*DeMets et al.*, 1994; *Chu and Gordon*, 1999; *Lemaux et al.*, 2002; *Horner-Johnson et al.*, 2005]. This region of the SWIR formed since ~64 Ma due to the north-eastward propagation of the Rodriguez Triple Junction [e.g., *Patriat and Courtillot*, 1984; *Patriat and Segoufin*, 1988], and has been separated into 3 sections on the basis of mean axial depth and ridge obliquity [*Cannat et al.*, 1999; *Sauter et al.*, 2001].

[9] 1. Between the Indomed and Gallieni transform faults (46°E–52°E), the ridge trends 070°N and has a mean axial depth of 3090 m. Geochemical analyses of basalts suggest the largest degree of partial melting along the eastern SWIR [*Meyzen et al.*, 2003] and a crustal thickness of ~6 km [*Cannat et al.*, 1999]. Segmentation of the ridge axis between 49°E and the Gallieni transform fault has been defined by *Cannat et al.* [1999] on the basis of variations in along-axis depth and MBA. Bathymetric segments have an average length of 64 km, but two large (>30 mgal) MBA lows have a spacing of ~120 km.

[10] 2. Between the Gallieni and Melville transform faults (52°E–61°E) the ridge trends at 045°N, and is characterized by bathymetrically defined second-order segments with an average length of ~70 km, which correlate well with gravimetric segments defined by the MBA in this region [*Cannat et al.*, 1999; *Rommevaux-Jestin et al.*, 1997]. The second-order segments are separated by relatively large spreading-parallel ridge-offsets and the fracture zones that extend from these offsets define a crenulated off-axis terrain [*Phipps Morgan and Parmentier*, 1995; *Patriat et al.*, 1997; *Sandwell and Smith*, 1997] (Figure 1). The mean axial depth is 4330 m [*Cannat et al.*, 1999], while chemical and seismic data suggest a relatively uniform crustal thickness of ~4 km [*Muller et al.*, 1997].

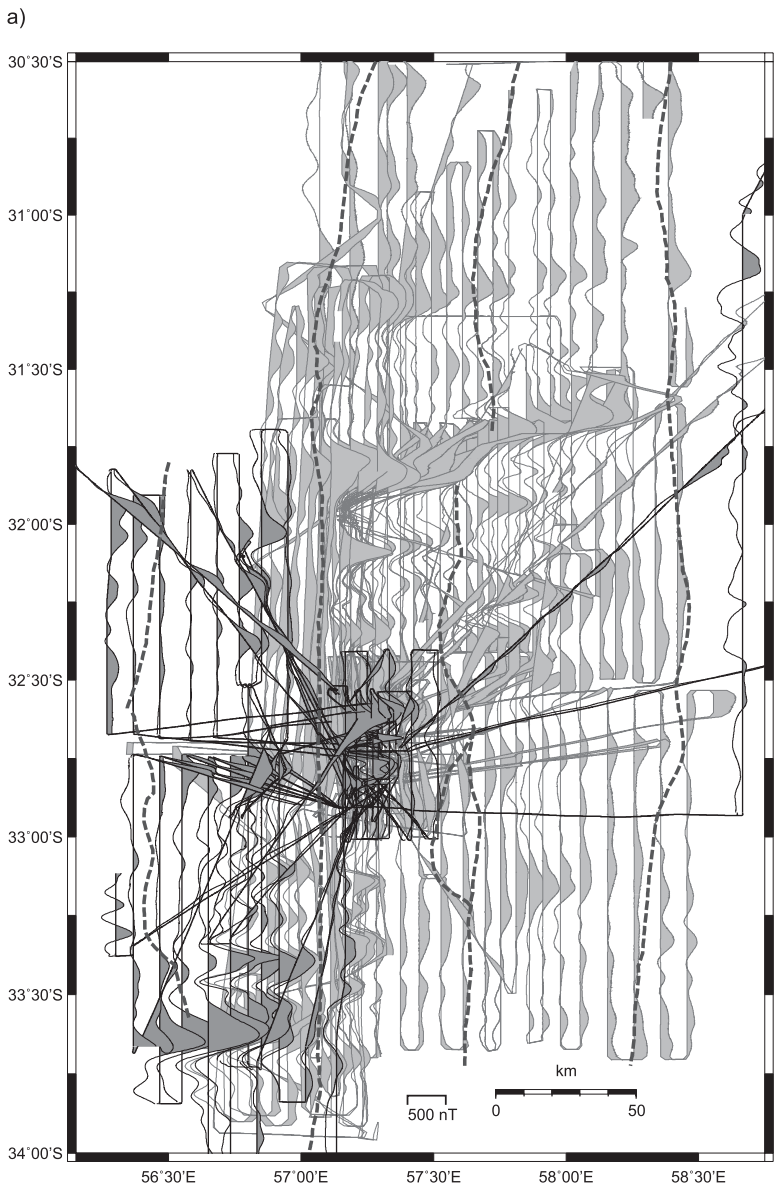

Figure 4. (a) Total magnetic field anomaly plotted along track lines. Data from the YK01-14 cruise are shown by black track lines and dark gray shading of positive anomalies; data from previous cruises [*Hosford et al.*, 2003] are shown using gray lines with light gray shading of positive anomalies. Thick-dashed lines show the trend of fracture zones in the area. (b) Gridded crustal magnetization solution: black lines, normal isochrons; white lines, reversed isochrons. (c) Crustal magnetization extracted on selected north-south track lines. Note that at these slow spreading rates the isochrons C5ACn and C5ADn merge to form a single identifiable anomaly. Here this anomaly is labeled as C5ADn because the age of this chron is 14.2 Ma, which corresponds to the beginning of chron C5ADn.

[11] The spreading-parallel ridge offsets in this section of the ridge have two potential origins: (1) they developed after the ridge had formed in response to a subsequent change in plate spreading direction thereby allowing the individual ridge segments to realign perpendicular to the spreading direction [*Patriat et al.*, 1997] or (2) they developed during triple junction migration, for example during an unstable phase of triple junction migration rather than the stable propagation of a ridge-ridge-ridge triple junction that is likely to have dominated [*Patriat and Courtillot*, 1984; *Dyment*, 1993].

[12] 3. Between the Melville transform fault and the Rodriguez Triple Junction (61°E–70°E), the SWIR trends 085°E, has a mean axial depth of

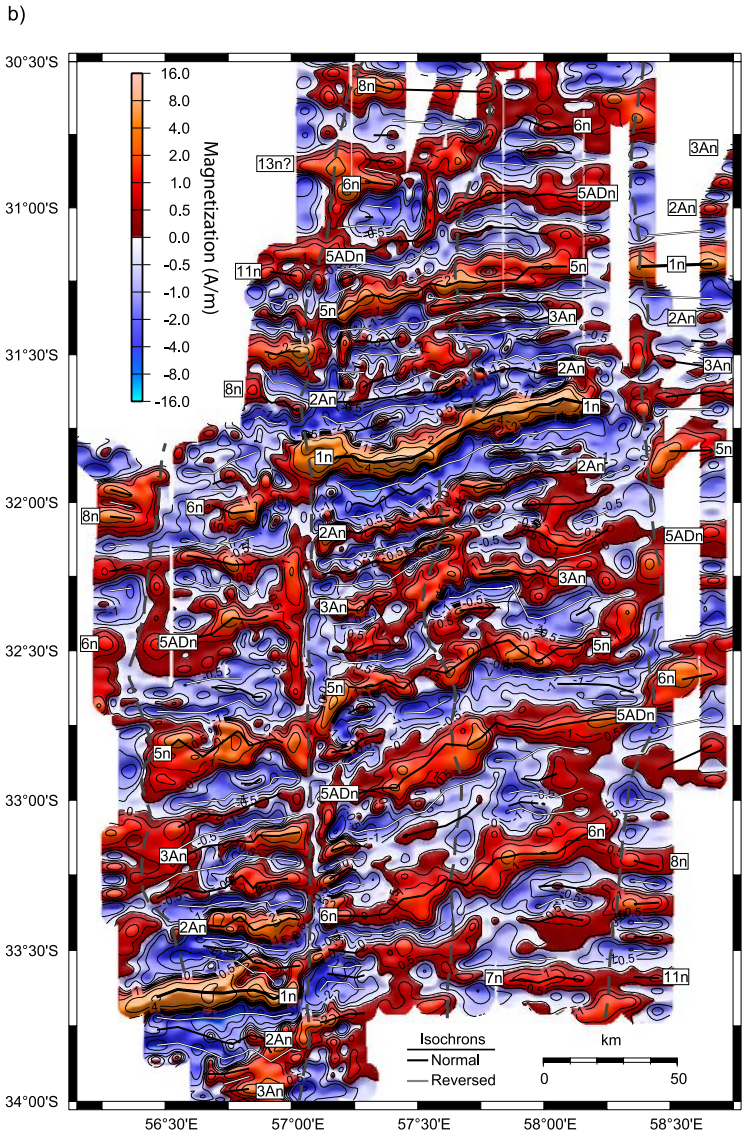

Figure 4. (continued)

4730 m and basalt geochemistry implies a low degree of partial melting, suggesting an average crustal thickness of 2.7 km and an underlying mantle that is 80°C cooler than west of the Gallieni transform fault [*Cannat et al.*, 1999; *Meyzen et al.*, 2003]. Results of a seismic refraction experiment located at ~66°E suggest that crustal thickness is highly variable (2–6 km) with a local mean thickness of 4 km [*Muller et al.*, 1999]. In contrast to the area between the Gallieni and Melville Transform Faults, the pattern of along-axis segmentation is irregular. Segments of ~50 km length are defined by along-axis bathymetry which correlates poorly with the MBA suggesting that the bathymetric highs are uncompensated and that the lithosphere here is relatively cold and thick [*Rommevaux-Jestin et al.*, 1997]. Both the along-axis bathymetry and the MBA are dominated by three segments that have significant along-axis relief and large (>40 mgal) negative MBAs [*Patriat et al.*, 1997; *Cannat et al.*, 1999]. These large bathymetric highs, for example at 61°30′E (Figure 1b and Figure 4), are thought to be large volcanic constructs that fill the axial valley at segment centers. *Cannat et al.* [2003] infer that melt distribution is more focused and variable than at the MAR or elsewhere on the SWIR and that transient melt focusing events led to the formation of the observed volcanic constructs. Away from these constructs, in areas of very low melt supply "smooth seafloor" forms [*Cannat et al.*, 2006]. This smooth seafloor represents a (nearly) avol-

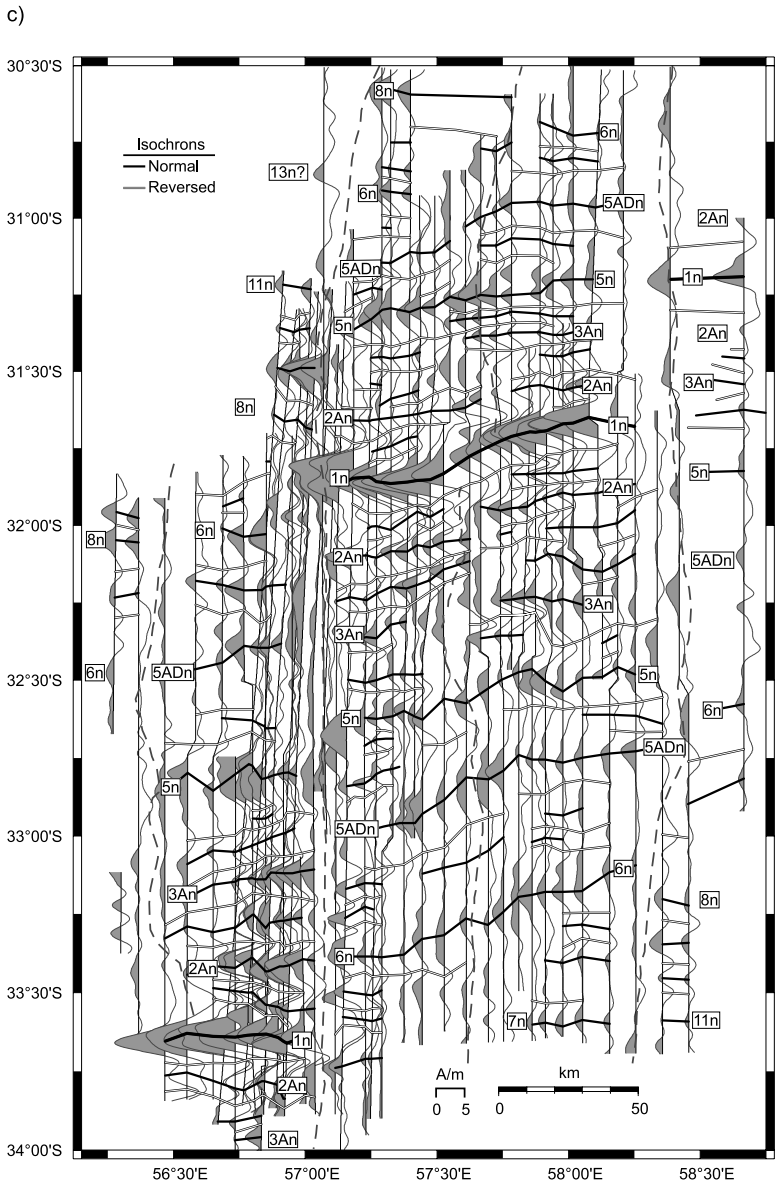

Figure 4. (continued)

canic end-member to plate spreading that is specific to melt-poor ultraslow-spreading ridges.

3. Segment Nomenclature

[13] Three different naming schemes have been presented for axial segmentation along the eastern SWIR (Table 2); these schemes differ significantly, in particular with regard to their treatment of oblique amagmatic spreading segments. *Rommevaux-Jestin et al.* [1997] include some oblique amagmatic spreading segments within their scheme; they use the prefix S and number the segments eastward starting at the 56°30′E nontransform discontinuity and extending to the Rodriguez Triple Junction. In contrast, *Cannat et al.* [1999] use a sequential numbering system that increases westward starting at the RTJ and extending to 49°E, oblique amagmatic spreading segments are not included as spreading segments but are referred to as a class of nontransform discontinuities. From 57°E–58°45′E, *Hosford et al.* [2003] name the spreading segments using the initials of the nearest transform faults and then numbering the intervening segments (from west to east). In this scheme, the two segments between the Atlantis II and Novara transform faults are both given the prefix AN, where the western segment is called AN-1, and the segment to the east

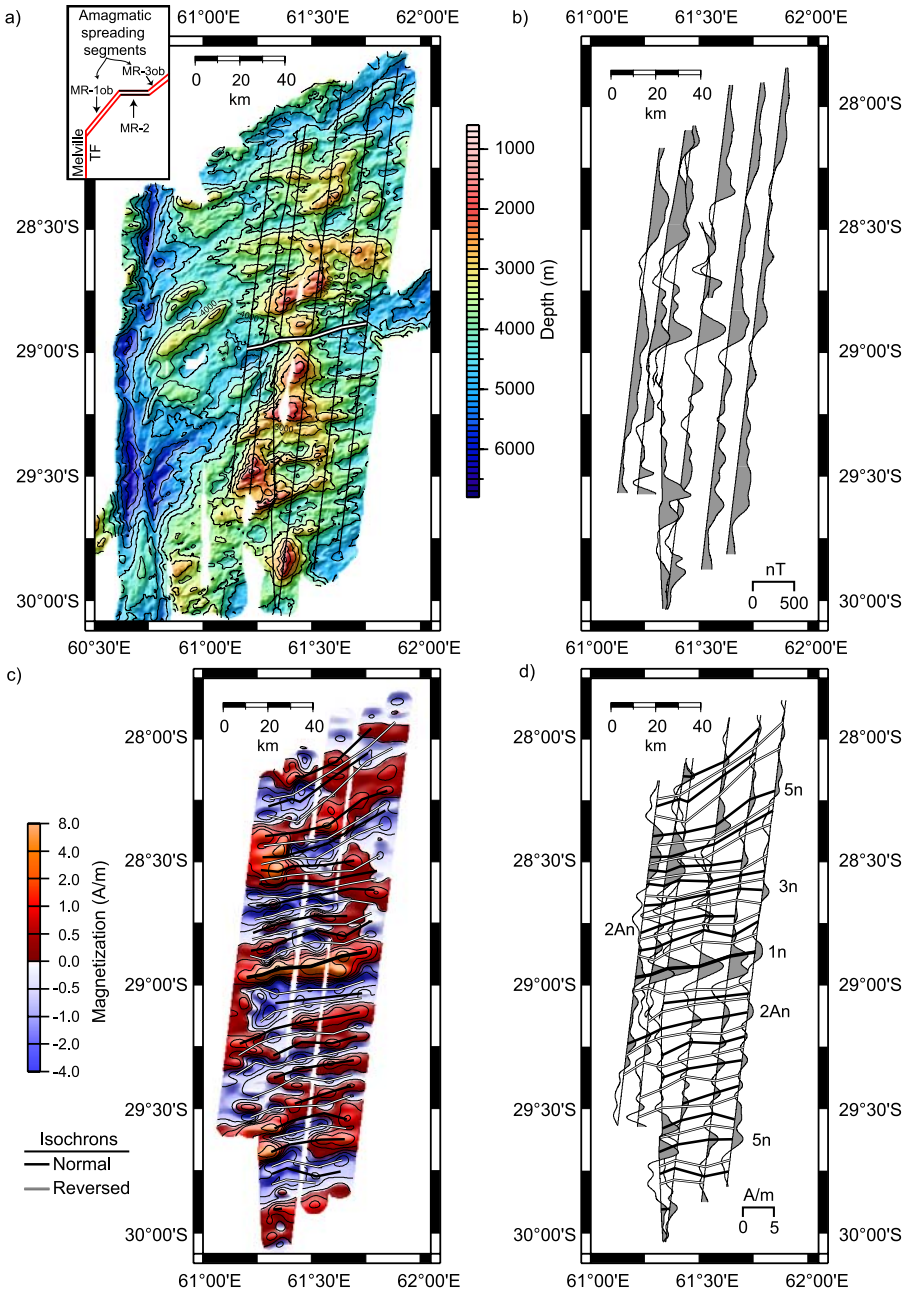

Figure 5. Segment MR-2. (a) Multibeam bathymetry west of the Melville Fracture Zone. Grid is composed of data from *Mendel et al.* [1997] and *Arai et al.* [2001]. Uses the same color scale as Figure 2. Note the oblique trend of the abyssal hills on either side of segment MR-2. Inset shows a cartoon of the ridge geometry and nomenclature. (b) Total magnetic field anomaly along track lines from *Arai et al.* [2001]. (c) Gridded crustal magnetization solution. (d) Crustal magnetization extracted on track lines.

is termed AN-2. Also the segment, immediately to the east of the Novara transform fault is given the name NM-1 (where the initial M refers to the Melville Transform fault).

[14] There is some inconsistency between naming conventions especially with regard to the classification of oblique amagmatic spreading segments. Although oblique amagmatic segments offset magmatic segments in the significant spreading-parallel direction, unlike nontransform discontinuities and transform faults they also extend the ridge-axis perpendicular to spreading and thus create new oceanic lithosphere. In view of the latter, we use a segment nomenclature that includes all accretionary

Table 1. Full-Spreading Rates and Azimuths at the SWIR, Using the Published Poles of Rotation[a]

		Indomed 46°06′E 39°30′S		Gauss 54°05′E 35°05′S		Atlantis II 57°06′E 32°45′S		Novara 58°24′E 31°30′S		Melville 60°45′E 30°00′S		RTJ 70°00′E 25°30′S	
Source	Time, Ma	Rate	Azimuth	Rate	Azimuth	Rate	Azimuth	Rate	Azimuth	Rate	Azimuth	Rate	Azimuth
NUVEL1A	0–3	14.1	353	14.1	357	14.0	359	13.9	359	13.9	000	13.3	357
Horner-Johnson et al. [2005]	0–3.2	14.7	006	14.5	002	14.4	001	14.3	000	14.2	001	13.4	003
Patriat and Segoufin [1988]	0–19.7	15.0	004	14.5	000	14.2	000	14.0	000	13.8	001	12.5	002
	19.7–39.5	22.8	011	22.1	008	21.8	007	21.7	007	21.4	006	20.0	005
	39.5–63.1	21.8	359	23.0	353	23.4	351	23.5	350	23.8	348	24.5	343

[a] Rates are calculated using GPTS 2004. All rates are km/Myr, and azimuths are degrees east of north.

spreading segments, both oblique amagmatic spreading segments and magmatic spreading segments and refer to nontransform discontinuities, which do not extend the SWIR any appreciable distance perpendicular to spreading, simply by longitude. To avoid (potentially) confusing modifications to the nomenclatures of *Cannat et al.* [1999] and *Rommevaux-Jestin et al.* [1997], we adopt the nomenclature of *Hosford et al.* [2003] and apply it between the Gauss and Atlantis II transform faults and east of the Melville Transform Fault (Table 2) (Figure 2 and Figure 5). We identify oblique spreading segments using the suffix -ob and follow *Dick et al.* [2003], who subdivided segment 20 of *Cannat et al.* [1999] into two segments separated by an 11-km-wide nontransform discontinuity (segments GA-5 and GA-6).

4. Previously Determined Spreading Rates

4.1. 54°45′E–58°45′E

[15] The main focus of this study is the SWIR from 54°45′E to 58°45′E. This section of the SWIR has an overall trend of 045°N and comprises six orthogonal spreading segments and two oblique amagmatic spreading segments (Table 2); it is offset parallel to spreading by two transform faults (Atlantis II and Novara) and two nontransform discontinuities (at 56°30′E and 57°40′E) (Figure 2). Previous analyses of spreading rates from subregions of this area have been presented by *Dick et al.* [1991], *Hosford et al.* [2003], and *Mendel et al.* [2003]. For segments GA-3 and GA-5, spreading rates have been approximately symmetric since 11 Ma [*Mendel et al.*, 2003; *Sauter et al.*, 2004]. For GA-3, they are 6.9 km/Myr north and 7.0 km/Myr south, while for GA-5 they are 6.9 km/Myr to the north and 6.8 km/Myr to the south. Although data were collected over segments GA-2ob and GA-4ob, magnetic anomalies are poorly defined so spreading rates could not be determined.

[16] *Dick et al.* [1991] used data collected in a narrow swath either side of the Atlantis II transform fault to calculate half-spreading rates to the north of segment GA-6 and to the south of segment AN-1. They suggested asymmetric spreading and recognized three periods with distinct half-spreading rates both north of GA-6 and south of AN-1: (1) 9.4

Table 2. Segment Nomenclature

Longitude	Type	*Rommevaux-Jestin et al.* [1997]	*Cannat et al.* [1999]	*Dick et al.* [2003]	*Hosford et al.* [2003]	This Paper
54°33′E–55°05′E	amagmatic					GA-2ob
55°05′E–55°28′E	magmatic		21	21		GA–3
55°28′E–55°55′E	amagmatic					GA-4ob
55°55′E–56°25′E	magmatic		20	20a		GA-5
56°25′E–57°05′E	magmatic	S1	20	20b		GA-6
57°08′E–57°40′E	magmatic	S2	19		AN-1	AN-1
57°40′E–58°20′E	magmatic	S3	18		AN-2	AN-2
58°25′E–59°02′E	magmatic	S4	17		NM-1	NM-1
60°46′E–61°13′E	amagmatic	S8				MR-1ob
61°13′E–61°45′E	magmatic	S9	14			MR-2
61°45′E–62°10′E	amagmatic	S10				MR-3ob

km/Myr from C1n–C5Cn (0–10.4 Ma), (2) 5.7 km/Myr from C5Cn –C7n (10.4–24.3 Ma), and (3) 11.1 km/Myr from C7n–C10n (24.3–29.1 Ma). These rates have been recalculated from those presented by *Dick et al.* [1991] using the geomagnetic polarity time-scale 2004 (GPTS 2004) [*Ogg and Smith*, 2004] rather than that of *Kent and Gradstein* [1986]. Given a full-spreading rate of 14 km/Myr, these half-spreading rates imply highly asymmetric spreading.

[17] Conversely, *Hosford et al.* [2003] suggested the half-spreading rates for segments AN-1 and AN-2 have been nearly constant for the past 25 Ma at 8.5 km/Myr to the south and 5.5 km/Myr to the north. Both *Hosford et al.* [2003] and *Dick et al.* [1991] report long periods of asymmetric spreading that likely resulted in major changes in the geometry of the ridge axis. Fast-to-the-north spreading west of the Atlantis II transform fault combined with fast-to-the-south spreading east of the transform imply that it has been growing at >3 km/Myr for at least the past 15 Ma. Also comparing *Mendel et al.*'s [2003] spreading rates for segment GA-5 to *Dick et al.*'s [1991] for the eastern half of segment GA-6 would suggest that the intervening 11-km-long nontransform discontinuity at 56°30′E was previously longer than it is today. We have analyzed newly acquired data from cruise YK01-14 together with the previously published data from 56°15′E to 58°45′E to constrain these changes in plate-boundary, and present the first integrated synthesis of spreading rates from 54°45′E–58°45′E along the SWIR.

4.2. 61°E–62°E

[18] During the R/V *Karei* KR00-06 cruise to Atlantis Bank [*Arai et al.*, 2001] data were collected across a magmatic spreading segment between 61°13′E and 61°45′E (Figure 5); this segment is referred to here as segment MR-2 (Table 2). Unlike much of the SWIR east of the Melville Transform Fault, segment MR-2 is shallow, the axial valley shoals to <3000 m (compared to the average 4730 m [*Cannat et al.*, 1999]), and has a high-amplitude central magnetic anomaly and a large negative MBA [*Patriat et al.*, 1997]. Together these data suggest that this segment is magmatically robust and that the crust will record magnetic anomalies that allow the history of plate spreading to be determined. Previous analysis of the spreading history of segment MR-2 has been limited, *Cannat et al.* [2006] presented anomaly picks for this segment and the entire SWIR east of ~61°E, but did not present a detailed analysis of spreading rates determined from those picks. Here we present a detailed analysis for segment MR-2.

[19] Both of the segments adjacent to MR-2 (MR-1ob and MR-3ob) are oblique to the spreading direction and the central magnetic anomaly and the MBA in these segments are of much lower magnitude [*Patriat et al.*, 1997]. These observations are consistent with other oblique amagmatic spreading segments [*Dick et al.*, 2003] so we suggest that this section of the ridge is comparable to that observed further west between 54°30′E and 56°E (Figure 2). However, a significant difference is that segment MR-1ob, which trends to the southwest for ~70 km, extends the ridge ~45 km perpendicular to the spreading direction and offsets it ~55 km parallel to the spreading (Figure 5a), is terminated to the west by the Melville Transform Fault. A similar geometry is observed at 9°E–16°E on the SWIR where an oblique amagmatic spreading segment is bounded to the west by the Shaka Transform Fault [*Dick et al.*, 2003]. These relationships clearly show that oblique amagmatic spreading segments can coexist with, as well as replace, transform faults at ultraslow-spreading ridges.

5. Magnetic Data

[20] The recent JAMSTEC R/V *Yokosuka* YK01-14 cruise to the Atlantis Bank [*Matsumoto et al.*, 2002] collected multibeam bathymetric and magnetic data west of the Atlantis II transform fault to extend data collected on previous JAMSTEC cruises and cruise RC2709 of the R/V *Robert Conrad* (Figures 2 and 4) [*Hosford et al.*, 2003]. The primary aim of YK01-14 was to conduct a manned submersible dive program at Atlantis Bank. In addition to the successful dive program [*Matsumoto et al.*, 2002], a geophysical program was undertaken over night and when weather conditions or scheduled maintenance did not allow submersible operations. Multibeam bathymetry, underway magnetic and continuous GPS navigation data were collected west of the Atlantis II transform fault and an additional line was collected east of the Novara transform fault (Figure 4a). Multibeam bathymetry data were collected using the SeaBeam 2100 system, and gridded using the MB-System [*Caress and Chayes*, 1996] and Generic Mapping Tools software [*Wessel and Smith*, 1998]. The bathymetry data were then combined with data from previous cruises [*Hosford et al.*, 2003; *Sauter et al.*, 2001; *Mendel et al.*, 1997] and satellite-derived bathymetry data [*Smith and Sandwell*, 1997] to produce the grid plotted in Figure 2.

[21] Total magnetic field data were recorded using a surface-towed proton precession magnetometer during YK01-14. The magnetometer was towed 400 m behind the GPS antenna and logged at 20 s intervals. Following onboard preprocessing to correct the location of the magnetometer, the ninth generation International Geomagnetic Reference Field (International Association of Geomagnetism and Aeronomy, 2003) was removed from the total force data to give the total force anomaly. Root-mean square error for 315 crossover points during the YK01-14 was 23 nT, which is less than daily secular variation and less than 2% of the total range of the anomaly data. Crossover error is most likely due to daily secular variation and errors in locating the towed magnetometer.

[22] The total magnetic field anomaly data from YK01-14 have been combined with data from three previous cruises [*Hosford et al.*, 2003] (Figure 4). Crossover analysis had already been conducted for the previous cruises [*Hosford et al.*, 2003] yielding a root-mean square (rms) error of 33 nT for 409 cross-ties. The root-mean square crossover error for the combined data set was 43.7 nT. Application of a constant 46 nT shift to the YK01-14 data reduced the RMS crossover error to 31 nT. Crossover error was further reduced to 23 nT by performing least squares error minimization following the method of *Prince and Forsyth* [1984].

[23] Bathymetry in the region varies by almost 6000 m so to correct for this variation in the depth of the magnetic source layer and for the skewness of the anomaly due to latitude, the magnetic field anomaly data (Figure 4a) were gridded and then inverted for crustal magnetization using the method of *Parker and Huestis* [1974] as extended for grids by *Macdonald et al.* [1980] (Figures 4b and 4c). The anomaly was gridded using a minimum curvature algorithm [*Smith and Wessel*, 1990] on an anisotropic grid. Given that the sampling rate is greatest along track lines (every ~100 m dominantly north-south) and ship tracks are more widely spaced east-west (1–7 km), we created a magnetic anomaly grid following *Weiland et al.* [1996], with higher resolution (0.5 nautical miles) along track lines than across track lines (1 nautical mile). For the inversion, this grid was resampled onto an isotropic grid with 0.5 nautical mile resolution. The Fourier-transform based inversion requires several assumptions: (1) a constant regional magnetic field direction, which was defined using the ninth generation IGRF assessed at the center of the surveyed area, (2) a constant thickness magnetic source layer that follows bathymetry and is uniformly magnetized with depth, and (3) a fixed nonvarying direction of crustal magnetization. In order to ensure convergence of the inversion solution, a band-pass filter was applied to the total force anomaly data with cosine tapers from 3.5 km to 7 km and 50–100 km.

[24] Often sediment thickness data are required to perform such an inversion, but in the study region, thick (up to 900 m) sediment cover is limited to transform fault valleys and to the traces of non-transform discontinuities. These areas comprise a small portion of the study region and the thickness of sediment cover as determined by seismic reflection data, away from these depressions is not significant [*Muller et al.*, 2000]. Therefore we have not included a sedimentary layer in our inversions.

[25] Constraints on the thickness of the magnetic source layer in oceanic crust are relatively limited. While many studies have concluded that the magnetic source layer is confined to the upper 500 m of extrusive crust [e.g., *Talwani et al.*, 1971], others have concluded that the lower crust and/or serpentinized upper mantle may contribute significantly to observed magnetic anomalies, especially at slower spreading ridges [e.g., *Fox and Opdyke*, 1973; *Dick et al.*, 1991; *Kikawa and Pariso*, 1991; *Dyment et al.*, 1997; *Nazarova et al.*, 2000; *Worm*, 2001; *Hosford et al.*, 2003]. In our study area, paleomagnetic analyses of gabbro recovered from ODP hole 735B (at 57°17′E 33°43′S on Atlantis Bank [*Shipboard Scientific Party*, 1989]) show the average natural remanent magnetization is 2.5 A/m (1.9 A/m with a geometric mean), with no decrease in magnetization down the 1508 m of the hole [*Worm*, 2001; *Natland and Dick*, 2002]. These magnetization data together with the linear magnetic anomalies observed over Atlantis Bank suggest that gabbroic lower crust is a good magnetic source layer in this region [*Dick et al.*, 1991; *Kikawa and Pariso*, 1991; *Worm*, 2001]. No other constraints on source layer thickness are available in the region, so we use the data from Hole 735B and assume a 1.5-km-thick magnetic source layer. Varying the thickness of the magnetic source layer generally has a minor effect; for example, assuming a layer thickness to 500 m [see *Hosford et al.*, 2003] has the effect of increasing the amplitude of magnetization, but the pattern of magnetization is only slightly modified.

[26] In the inversion, we assume that the inclination of crustal magnetization matches that of a geocentric dipole (−51°). However, at Atlantis Bank, paleomagnetic data from ODP Hole 735B record an average inclination of −71° [*Natland*

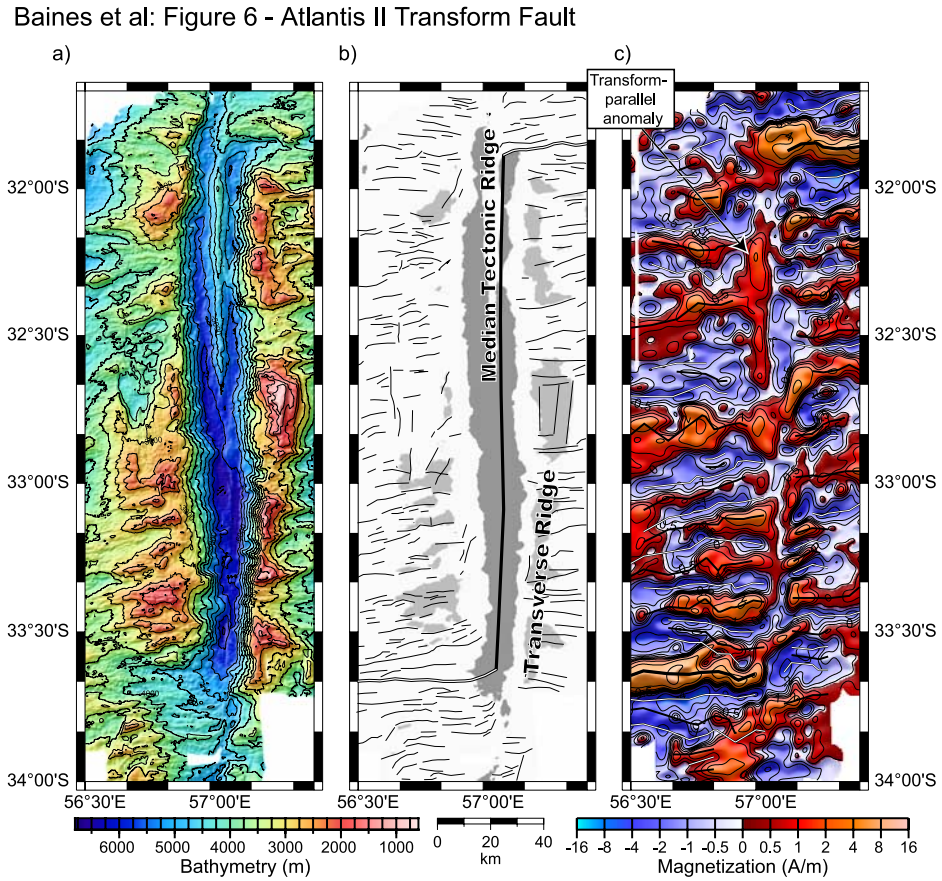

Figure 6. The Atlantis II transform valley. (a) Bathymetry. (b) Structural interpretation. Bathymetry shallower than 2500 m shaded light gray, and bathymetry deeper than 5000 m shaded dark gray. (c) Crustal magnetization: black lines, normal isochrons; white lines, reversed isochrones.

and Dick, 2002] and oriented shallow drill cores reveal a similar magnetic inclination [*Allerton and Tivey*, 2001]. Given the inclination of a geocentric dipole at this latitude (−51°), these data imply >20° of tectonic rotation below the Curie temperature (500–580°C [*Worm*, 2001]). However, because Atlantis Bank is an oceanic core-complex and represents a small, anomalous subsection of the study area, this tectonic rotation cannot be inferred to have affected entire region, so we use an inclination of crustal magnetization parallel to the geocentric dipole.

[27] Magnetic data from segment MR-2 were analyzed in a similar manner to the above (Figure 5). However, due to the wider spacing between track lines, the total force magnetic anomaly was initially gridded using an anisotropic grid with 0.5 nautical mile resolution along track lines and 2 nautical mile resolution across track lines.

[28] The magnetization solutions for both areas (Figures 4b and 4c and Figures 5c and 5d) show ridge-parallel magnetic anomalies. Often, an annihilator is used to balance the amplitude of the positive and negative anomalies away from the central Brunhes anomaly in an inverse solution. An annihilator is a magnetization distribution for the magnetic source layer that produces no external field at the observation level. The addition of any multiple of the annihilator produces a nearly constant shift to the magnetization amplitudes and so allows the amplitude of anomalies to be balanced. Addition of an annihilator was not required for either study area because positive and negative anomalies away from the central Brunhes anomaly are of equal magnitude. The ridge-parallel anomalies have been correlated with GPTS2004 [*Lourens et al.*, 2004; *Ogg and Smith*, 2004] and used to determine the half-spreading rates for each segment (see below).

[29] In addition to the ridge-parallel anomalies, a large north-south trending positive magnetic anomaly is observed both in the total force anomaly (>200 nT; Figure 4a) and crustal magnetization (>2 A/m;

Figure 6c) over the Atlantis II Transform valley. This anomaly overlies a 100-km-long median tectonic ridge (Figure 6b). *Dick et al.* [1991] inferred that uplift of this ridge is due to low-density serpentinites that formed when peridotite was exposed within the transform fault valley during a long-lived period of transtension following the 10° rotation in plate spreading direction during C6n (~19 Ma). More recently serpentinized peridotite has been found at depths of 3–4 km on the western margin of Atlantis Bank [*Arai et al.*, 2001; *Kinoshita et al.*, 2001; *Matsumoto et al.*, 2002] and *Muller et al.* [2000] used seismic velocity data to suggest that the crust within the transform valley is predominantly serpentinized peridotite. Therefore the observed magnetic anomaly over the median tectonic ridge may be attributed to a stable chemical remanent magnetization acquired during serpentinization [*Lienert and Wasilewski*, 1979; *Arkani-Hamed*, 1988; *Shive et al.*, 1988; *Bina and Henry*, 1990; *Krammer*, 1990; *Nazarova*, 1994; *Nazarova et al.*, 2000; *Dyment et al.*, 1997]. We note that a similar explanation has been proposed for a positive transform-parallel magnetic anomaly observed over the transform-parallel Blanco Ridge on the Juan de Fuca Ridge [*Dziak et al.*, 2000].

6. Spreading Rates

[30] Spreading rates have been determined by correlating ridge-parallel magnetic anomalies to the GPTS 2004 [*Ogg and Smith*, 2004]. Magnetic isochrons were handpicked at peaks and troughs in the solutions for crustal magnetization (Figures 4c and 4d and Figures 5c and 5d), and ages for these isochrons were defined as the midpoint of the corresponding polarity epoch. In general, only polarity epochs of long duration (~300 kyr) could be confidently identified because ultraslow-spreading rates lead to a compressed time-scale and because of the effect of upward continuation to sea level. One consequence of this is that chrons C5ACn and C5ADn merge to form a single identifiable anomaly. For convenience, we refer to this anomaly as C5ADn because the midpoint of the combined anomaly is 14.2 Ma, equivalent to the beginning of chron C5ADn.

[31] Synthetic magnetization profiles generated using the GPTS 2004 were used to refine and verify our magnetic isochron picks (Figure 7). Most observed profiles compare well to synthetic profiles generated assuming constant half-spreading rates over time and minor discrepancies between the locations of the synthetic and observed anomalies reveal short-lived perturbations in half-spreading rates that are discussed in more detail below. The exception is segment NM-1 where synthetic profiles that assume a constant half-spreading rate are a poor match to the observed profile of crustal magnetization. A much better fit is obtained by a synthetic profile generated using a simple two-phase spreading model with different half-spreading rates before and after 15.6 Ma (C5Br) (10.6 km/Myr and 6.8 km/Myr, respectively) (Figure 7d).

[32] The spreading rates reported below and in Table 3 are best-fit spreading rates determined by linear bivariate regression [*York*, 1966] through the handpicked anomaly data (Figures 4b and 4c and Figures 5c and 5d). Two-sigma errors (95% confidence) on the best-fit spreading rates have been calculated using this method and are largely dependent on the time interval over which rates are determined; generally, the longer the interval under consideration the lower the error (Table 3). For example, errors on spreading rates determined over ~10 Myr (median error is 0.3 km/Myr) are approximately half those on rates determined over 5–6 Myr (a median error of 0.6 km/Myr). We note that plots of distance against time (Figure 8) suggest variations in spreading rates over time periods of less than 5 Myr; and that in certain areas, for example around Atlantis Bank, it is possible to determine accurate spreading rates over periods <5 Myr [*Baines et al.*, 2005]. However, generally, errors are large on rates determined over periods <5 Myr, so here we restrict our discussion to spreading rates determined over periods ≥5 Myr and between well-constrained magnetic isochrons.

[33] Previously reported regional full-spreading rates for the SWIR provide additional constraints on the spreading rates we have determined. The NUVEL1A plate-motion model [*DeMets et al.*, 1994] suggests plate-spreading between the African and Antarctic plates is directed approximately north-south, and that the full-spreading rate decreases slightly to the east from ~14.1 km/Myr at the Indomed transform fault to 13.3 km/Myr at the Rodriguez Triple Junction (Table 1). Recent studies have split the African plate into two component plates, the Nubian and Somalian plates [*Chu and Gordon*, 1999; *Lemaux et al.*, 2002; *Horner-Johnson et al.*, 2005]. The boundary between these plates intersects the SWIR to the west of our study area, so the eastern SWIR forms the boundary between the Antarctic and Somalian plates. The pole of rotation between the Antarctic

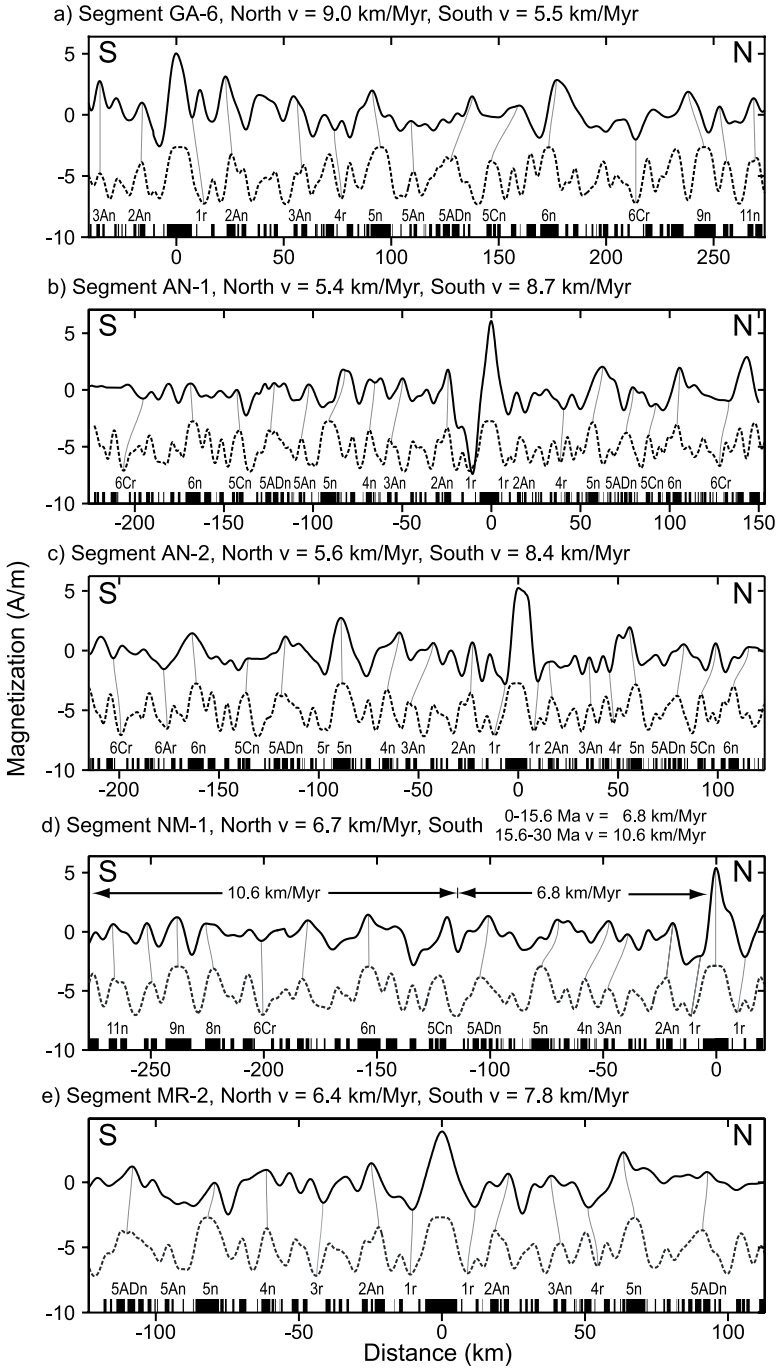

Figure 7. Representative profiles of crustal magnetization (solid lines) and synthetic profiles (dashed lines). Synthetic profiles were defined by applying a 2 km Gaussian filter to a function of magnetization with distance defined using the geomagnetic timescale and the time-averaged spreading rate [e.g., *Hosford et al.*, 2003].

and Somalian plates since C3An (6.4 Ma) [*Horner-Johnson et al.*, 2005] also suggests north-south spreading but at slightly faster full-spreading rates than NUVEL1A (Table 1). The full-spreading rates again decrease to the east from 14.7 km/Myr at the Indomed transform fault to 13.4 km/Myr at the RTJ. Full-spreading rates and azimuths since the start of C6n (19.7 Ma) calculated using the GPTS 2004 and the pole of rotation calculated by *Patriat and Segoufin* [1988] match those determined by NUVEL1A and *Horner-Johnson et al.* [2005]. In addition, observations from *Hosford et al.* [2003], *Mendel et al.* [2003], *Sauter et al.* [2004], and *Cannat et al.* [2006] suggest a ~14 km/Myr full-

Table 3. Spreading Rates Determined From Magnetic Data[a]

	All Data	1n–6n (0–19.2 Ma)	1n–5n (0–10.4 Ma)	5n–6n (10.4–19.2 Ma)	6n–12n (19.2–30.9 Ma)	1n–3r (0–5.6 Ma)	3n–5n (4.7–10.4 Ma)	5n–5Br (10.4–15.6 Ma)	5ADn–6n (14.2–19.2 Ma)	6n–8n (19.2–25.7 Ma)	8n–12n (25.7–30.9 Ma)
GA-5											
North	7.8 ± 0.1 (6.9[b])[c]	7.4 ± 0.3	6.9[b]	8.2 ± 0.5	6.6 ± 0.5					6.9 ± 0.9	
South	6.8[b]		6.8[b]								
Full	14.6(± 0.3) (13.7[b])[c]		13.8[b]								
Asymmetry	11%[d] (1%)[c]	6%[d]	<1%								
GA-6											
North	9.0 ± 0.1 (8.5 ± 0.2)[c]	9.2 ± 0.1	8.7 ± 0.1	10.6 ± 0.4	7.6 ± 0.5	8.4 ± 0.2	9.3 ± 0.4	11.4 ± 0.5	8.9 ± 0.8	6.0 ± 0.7	12.4 ± 0.8
South	5.5 ± 0.3					5.5 ± 0.3					
Full	14.5 ± 0.4 (14.0 ± 0.5)[c]					13.9 ± 0.5					
Asymmetry	29 ± 1%[c] (21 ± 3%)[c]	31%[d]				21 ± 3%					
AN-1											
North	5.4 ± 0.1	5.4 ± 0.1	5.6 ± 0.2	4.9 ± 0.3		6.5 ± 0.5	5.7 ± 0.5	5.5 ± 0.6	4.2 ± 0.5	6.4 ± 0.8	
South	8.7 ± 0.1	8.7 ± 0.1	8.6 ± 0.2	9.8 ± 0.3		8.2 ± 0.4	8.9 ± 0.7	10.4 ± 0.6	9.7 ± 0.6	6.6 ± 0.6	
Full	14.1 ± 0.2	14.1 ± 0.2	14.2 ± 0.4	14.7 ± 0.6		14.7 ± 0.9	14.6 ± 1.2	15.9 ± 1.2	13.9 ± 1.1	13.0 ± 1.4	
Asymmetry	−23 ± 1%	−23 ± 1%	−21 ± 2%	−33 ± 3%		−12 ± 4%	−22 ± 7%	−31 ± 6%	−40 ± 7%	−2 ± 7%	
AN-2											
North	5.4 ± 0.1	5.4 ± 0.1	4.6 ± 0.2	6.7 ± 0.4		4.7 ± 0.3	5.7 ± 0.4	8.0 ± 0.4	5.4 ± 0.6		
South	8.6 ± 0.1	8.6 ± 0.1	9.4 ± 0.3	8.3 ± 0.3		9.8 ± 0.5	7.6 ± 0.7	7.6 ± 0.4	9.2 ± 0.5	7.7 ± 0.7	
Full	14.0 ± 0.2	14.0 ± 0.2	14.0 ± 0.5	15.0 ± 0.7		14.5 ± 0.8	13.3 ± 1.1	15.6 ± 0.8	14.6 ± 1.1		
Asymmetry	−23 ± 1%	−23 ± 1%	−34 ± 4%	−11 ± 3%		−35 ± 6%	−14 ± 7%	3 ± 3%	−26 ± 7%		
NM-1											
North	6.7 ± 0.4					6.7 ± 0.6					
South	8.6 ± 0.2 (6.7 ± 0.4)[c]	7.3 ± 0.3	6.5 ± 0.3	8.9 ± 0.9	10.4 ± 0.2	6.3 ± 0.5	7.4 ± 0.6	8.2 ± 1.5	10.7 ± 1.7	10.8 ± 1.1	10.3 ± 0.4
Full	15.3 ± 0.6 (13.4 ± 0.8)[c]					12.9 ± 1.0					
Asymmetry	−23%[d] (0 ± 3%)[c]	−4%[d]				5%					
MR-2											
North	6.4 ± 0.2		6.2 ± 0.2			6.2 ± 0.4	6.3 ± 0.6	8.1 ± 2.5			
South	7.8 ± 0.1		7.9 ± 0.1			7.8 ± 0.4	8.3 ± 0.4	7.0 ± 1.4			
Full	14.2 ± 0.3		14.3 ± 0.3			14.0 ± 0.8	14.6 ± 1.0	15.1 ± 3.9			
Asymmetry	−10 ± 2%		−12 ± 2%			−11 ± 4%	−14 ± 5%	7 ± 20%			
All segments											
Full Rate	14.2 ± 0.3 (14.0 ± 0.1)[c]	14.1 ± 0.2	14.1 ± 0.2	14.8 ± 0.5		13.8 + 0.8	14.3 + 0.5	15.7 + 0.7	14.3 + 0.8		

[a] All rates are in km/Myr.
[b] Spreading rates from *Mendel et al.* [2003].
[c] Rates and asymmetries in parentheses are those calculated over the time interval where data are available from both ridge flanks.
[d] Asymmetry calculated assuming 14 km/Myr full-spreading rate.

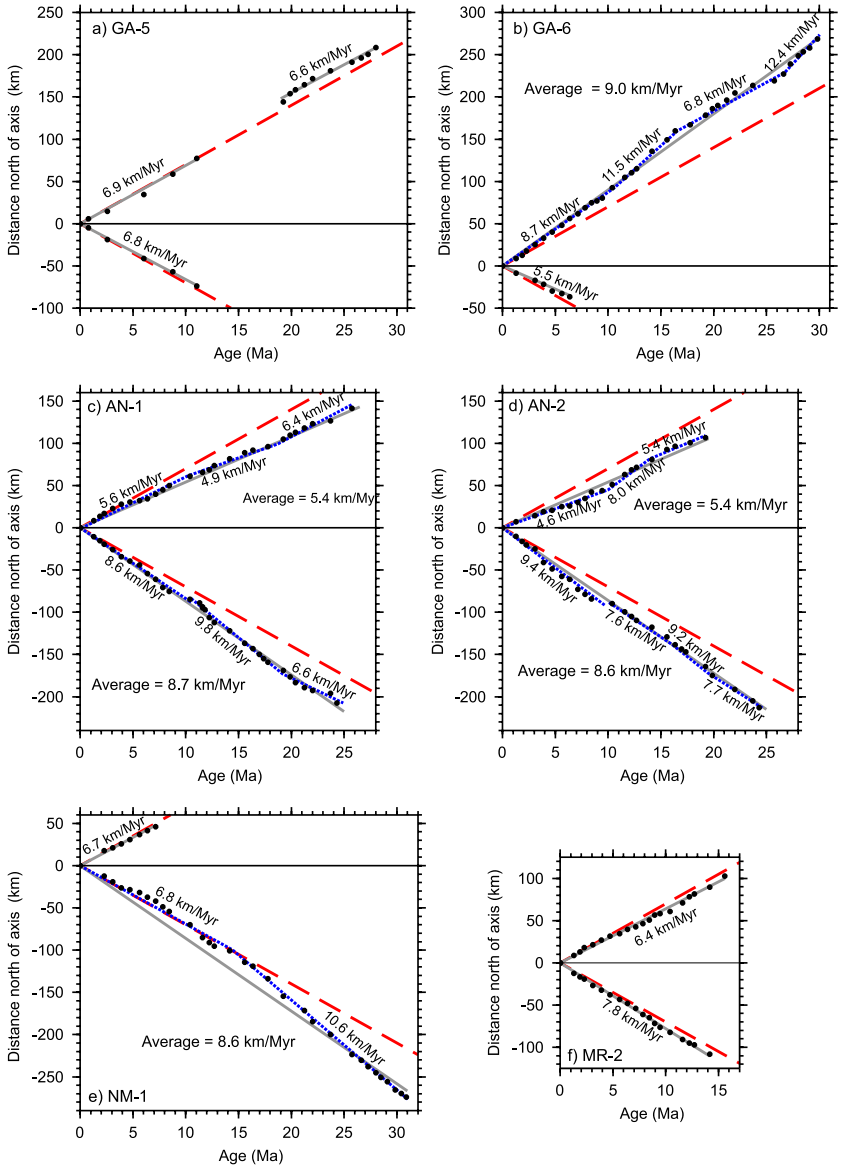

Figure 8. Distance-time plots for spreading segments considered in this study. Data from *Mendel et al.* [2003] (open circles) and from this study (filled circles). Solid gray lines are the lines of best fit through all the data determined by linear regression (with the intercept set at 0 km). Long red dashed lines represent the half-spreading rate assuming symmetric spreading (7 km/Myr). The relative slope of the gray lines to the red dashed lines provides an indication of the direction and magnitude of asymmetric spreading. Short blue dashed lines show half-spreading rates for subsets of the data as discussed in the main text.

spreading rate for the SWIR since at least 20 Ma. Hence, although there are differences, all the previous studies suggests that the full-spreading rate in our study area has been approximately 14 km/Myr since C6n (~19.2 Ma). The average full-spreading rates we calculate since C6n (Table 3) are also within error of 14 km/Myr, so where necessary in the following analysis we use this average 14 km/Myr full-spreading rate since C6n (19.2 Ma) to provide an estimate of spreading asymmetry when there are only data from one flank of the ridge axis.

[34] Prior to C6n, the regional full-spreading rates are poorly constrained. From C6n to C18n (19.2–39.4 Ma), the stage-poles calculated from *Patriat and Segoufin* [1988] suggest that the full-spreading rate was ~22 km/Myr (Table 1). *Cannat et al.* [2006] use data east of the Melville transform fault to infer a 16 km/Myr full-spreading rate from C6n to C6Cn (19.2–22.8 Ma) and, a significantly faster

(>30 km/Myr) full-spreading rate before C6Cn. We note that the change in full-spreading rate at C6n coincides with the 10° counterclockwise rotation in plate-spreading direction at this time (Figure 1) [*Hosford et al.*, 2003]. However, these full-spreading rates remain poorly constrained west of the Melville transform fault and as the majority of our data is over lithosphere younger than C6n, we do not to make assumptions about the full-spreading rate before C6n (19.2 Ma).

[35] We next discuss the spreading rates determined for individual magmatic segments from west to east. An important consideration in the following is that half-spreading rates and spreading asymmetry may vary significantly between adjacent spreading segments and result in the growth/reduction of intervening ridge offsets and relative ridge-migration. However, the full-spreading rates reflect the total rate of separation of the rigid Somalian and Antarctic plates and do not vary significantly between adjacent spreading segments.

6.1. GA-5

[36] Data collected during cruise YK01-14 along two track lines north of segment GA-5 allow the identification of magnetic isochrons C6n (19.2 Ma) to C9r (28.1 Ma). These data reveal a half-spreading rate of 6.6 ± 0.9 km/Myr, similar to the rate of 6.9 km/Myr obtained by *Mendel et al.* [2003] for C1n to C5r (0–12 Ma) (Table 3, Figure 8a). These similar rates suggest that the half-spreading rate to the north may have been approximately constant since 28.1 Ma and are consistent with the rates calculated by *Mendel et al.* [2003] since 12 Ma.

6.2. GA-6

[37] For segment GA-6, continuous magnetic profiles extend from the ridge-axis to C3An (6.4 Ma) south of the axis and to C11n (29.8 Ma) north of the axis. Data south of the axis suggest a half-spreading rate of 5.5 ± 0.3 km/Myr from C1n–C3An (0–6.4 Ma), while the half-spreading rate calculated to the north over the same interval is 8.5 ± 0.2 km/Myr. These half-spreading rates suggest a full-spreading rate of 14.0 ± 0.5 km/Myr from C1n–C3An, in agreement with the average full-spreading rate. The magnitude of spreading asymmetry since C3An is 21 ± 3%, where spreading asymmetry is defined as the half-spreading rate to the north minus the half-spreading rate to the south divided by the sum of the half-spreading rates. Using this definition, a negative value is obtained when spreading is fast-to-the-south.

[38] Data north of the ridge axis extend further off-axis and give a time-averaged half-spreading rate of 9.0 ± 0.1 km/Myr for the past 29.8 Myr. From C1n–C6n, the half-spreading rate is 9.2 ± 0.1 km/Myr, so spreading in this segment was asymmetric for at least 20 Myr (~31% assuming a 14 km/Myr full-spreading rate). In detail, four distinct periods of spreading since 29.8 Ma can be recognized (Figure 8b: dotted blue line): (1) Continuous linear anomalies out to C5n imply that the half-spreading rate to the north was 8.7 ± 0.1 km/Myr since 10.4 Ma, (2) from C5n to C5Cn (10.4–16.4 Ma) the half-spreading rate was faster at 11.5 ± 0.4 km/Myr, (3) from C5Cn to C8n (16.4–25.7 Ma) the rate was only 6.8 ± 0.3 km/Myr, and (4) before C8n (25.7 Ma) the half-spreading rate was 12.4 ± 0.8 km/Myr. Our interpretation is broadly consistent with that of *Dick et al.* [1991], the only significant difference is that we split the period from C1n–C5Cn into two sections but we note that the average half-spreading rate over this period is consistent with the interpretation of *Dick et al.* [1991].

6.3. AN-1

[39] For segment AN-1, data extend to C7n (24.3 Ma) south of the axis and to C8n (25.7 Ma) north of the axis. Average half-spreading rates of 8.7 ± 0.1 km/Myr to the south and 5.4 ± 0.1 km/Myr to the north imply greater spreading asymmetry (−23 ± 1%) than was reported by *Hosford et al.* [2003] (−21%). But we note that these discrepancies are small and can be explained by differences between GPTS 2004 and the timescale of *Cande and Kent* [1995] that was used by *Hosford et al.* [2003]. These time-scales differ by as much as 0.8 Myr from 15–30 Ma [*Lourens et al.*, 2004].

[40] In detail, there are subtle changes in spreading rate and spreading asymmetry over time (Figure 8c and Table 3). On a 10 Myr time-scale, half-spreading rates of 5.6 ± 0.2 km/Myr to the north and 8.6 ± 0.2 km/Myr to the south from C1n to C5n (0–10.4 Ma) are within error of the average half-spreading rates (Table 3), while from C5n to C6n (10.4–19.2 Ma) the half-spreading rates of 4.9 ± 0.3 km/Myr to the north and 9.8 ± 0.3 km/Myr to the south predict greater spreading asymmetry (−33%) and a faster full-spreading rate (14.7 ± 0.6 km/Myr). By examining the results over 5–6 Myr intervals it is clear that the increased full-spreading rate determined from C5n–C6n is due to a relatively short-lived increase in full-spreading rate (15.9 ± 1.2 km/Myr) from C5n to C5Br; we note that the increased full-spreading rate coincides

with the formation of the Atlantis Bank oceanic core-complex [*Baines et al.*, 2005].

6.4. AN-2

[41] For segment AN-2, data extend to C7n (24.3 Ma) south of the ridge-axis and to C6n (19.2 Ma) north of the ridge-axis. Time-averaged half-spreading rates are 5.6 ± 0.1 km/Myr to the north and 8.4 ± 0.1 km/Myr to the south, implying the same direction and magnitude (−23 ± 1%) of asymmetry as segment AN-1. However, when assessed over shorter time intervals, the spreading rates reveal a different pattern to that observed in segment AN-1.

[42] Over ∼10 Myr intervals, half-spreading rates of 4.6 ± 0.2 km/Myr to the north and 9.4 ± 0.2 km/Myr to the south from C1n–C5n require greater asymmetry (−34%) than rates of 6.7 ± 0.4 km/Myr to the north and 8.3 ± 0.3 km/Myr to the south from C5n–C6n (−11%), the opposite observation to segment AN-1. However, the calculated full-spreading rates show the same pattern as segment AN-1, with a faster full-spreading rate from C5n–C6n (15.0 ± 0.7 km/Myr). The spreading rates determined over 5–6 Myr indicate that this increased full-spreading rate is again due to a short-lived spreading rate increase from C5n–C5Br (to 15.6 ± 0.8 km/Myr). Though in contrast to segment AN-1 the spreading asymmetry in segment AN-2 is low (3 ± 3%) during this period of faster spreading.

6.5. NM-1

[43] For segment NM-1, the few available track lines extend from the ridge axis to C12n (30.9 Ma) south of the axis and to C3Ar (7.1 Ma) north of the axis. Over the period that data are available on both flanks of the ridge (0–7.1 Ma) they reveal symmetric spreading (6.7 ± 0.4 km/Myr in both directions) and a full-spreading rate within error of 14 km/Myr (Table 3). On the southern flank data extends further from the ridge axis and the simplest interpretation is that there were two periods with constant half-spreading rates. Before C5Br (15.6 Ma) the half-spreading rate to the south was ∼10.6 ± 0.2 km/Ma, while since that time the half-spreading rate was 6.8 ± 0.2 km/Myr. The half-spreading rates determined over shorter time intervals are within error of these half-spreading rates (Table 3), but we note that the half-spreading rates determined over 5–6 Myr intervals appear to have decreased steadily since C6n. The half-spreading rate was 10.7 ± 1.7 km/Myr from C5ADn–C6n (14.1–19.2 Ma), 8.2 ± 1.5 km/Myr from C5n–C5Br (10.4–15.6 Ma), 7.4 ± 0.6 km/Myr between C3n–C5n (4.7–10.4 Ma), and 6.3 ± 0.5 km/Myr from C1n to C3r (0–5.6 Ma). Before C5Br, a fast half-spreading rate (10.6 ± 0.2 km/Myr) to the south suggests that spreading was (up to 50%) asymmetric.

6.6. MR-2

[44] For segment MR-2 west of the Melville transform fault, data extend from the ridge axis to C5ADn (14.2 Ma) south of the axis and to C5Br (15.6 Ma) north of the axis. We note that the locations of our anomaly picks are consistent with those recently presented by *Cannat et al.* [2006]. The half-spreading rates determined using all the data are 6.4 ± 0.2 km/Myr to the north and 7.8 ± 0.1 km/Myr to the south, and so suggest that spreading was −10 ± 2% asymmetric, consistent with the maximum spreading asymmetry reported by *Cannat et al.* [2006]. Unlike other spreading segments analyzed above, all of the half-spreading rates determined over shorter time intervals are within error of these rates suggesting uniform half-spreading rates through time. However, we do note that the full-spreading rate determined from C5n–C5Br (15.1 ± 3.9 km/Myr) is consistent with the significantly faster full-spreading rates observed in segments AN-1 and AN-2 over the same period.

7. Paleoridge Geometry

[45] The full-spreading rates determined for each spreading segment are within error and consistent with the separation of rigid lithospheric plates. However, it is apparent that half-spreading rates and spreading asymmetry vary significantly between segments. These variations require that the length of intervening ridge offsets must have changed significantly, altering the shape of the plate-boundary. To illustrate this process, we use the spreading-parallel separation of magnetic isochrons between adjacent spreading segments as a proxy for the offset of the SWIR between individual ridge segments and plot the spreading-parallel offset across transform faults and nontransform discontinuities through time (Figure 9) [e.g., *Carbotte et al.*, 1991]. Additionally, we restore magnetic isochrons to the ridge axis using the spreading poles of *Patriat and Segoufin* [1988] and thus reconstruct the paleoridge geometry since C8n (25.7 Ma) (Figure 10).

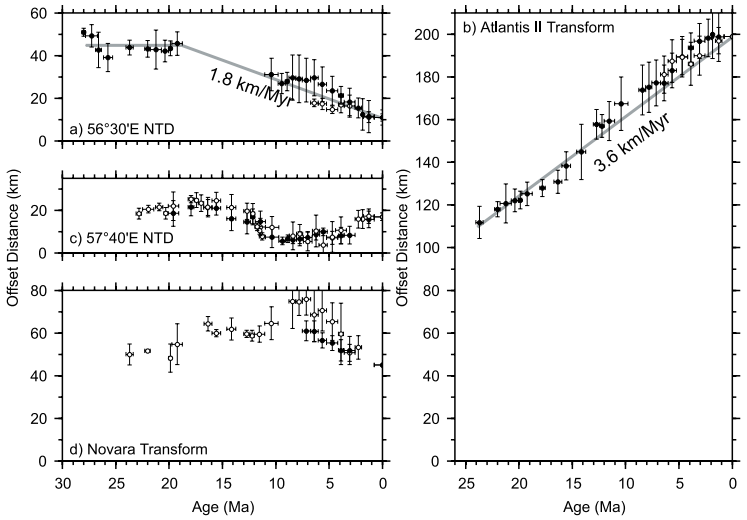

Figure 9. The spreading-parallel displacement of the SWIR across ridge offsets against time, determined from the offset of magnetic isochrons for (a) the 56°30′E nontransform discontinuity, (b) Atlantis II Transform Fault, (c) the 57°40′E nontransform discontinuity, and (d) Novara Transform Fault.

7.1. GA-4ob

[46] Near symmetric spreading of segments GA-3 and GA-5 [*Mendel et al.*, 2003] requires that segment GA-4ob has had a similar spreading-parallel offset since at least 11 Ma, indicating amagmatic spreading segments are a stable feature of ultraslow-spreading ridges that can persist for >11 Ma [*Dick et al.*, 2003]. Our data from the

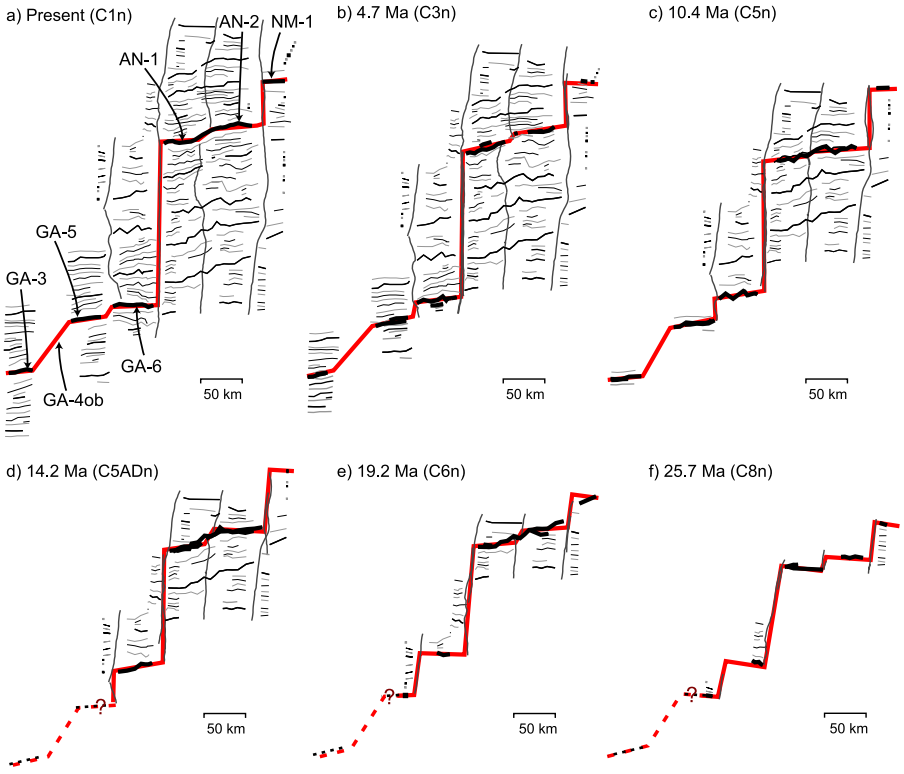

Figure 10. Evolution of the SWIR ridge from 54°45′E to 58°45′E for the past 26 Ma. Determined by rotating/backstriping isochrons shown in Figures 4b and 4c, back to the ridge axis using stage-poles calculated after *Patriat and Segoufin* [1988].

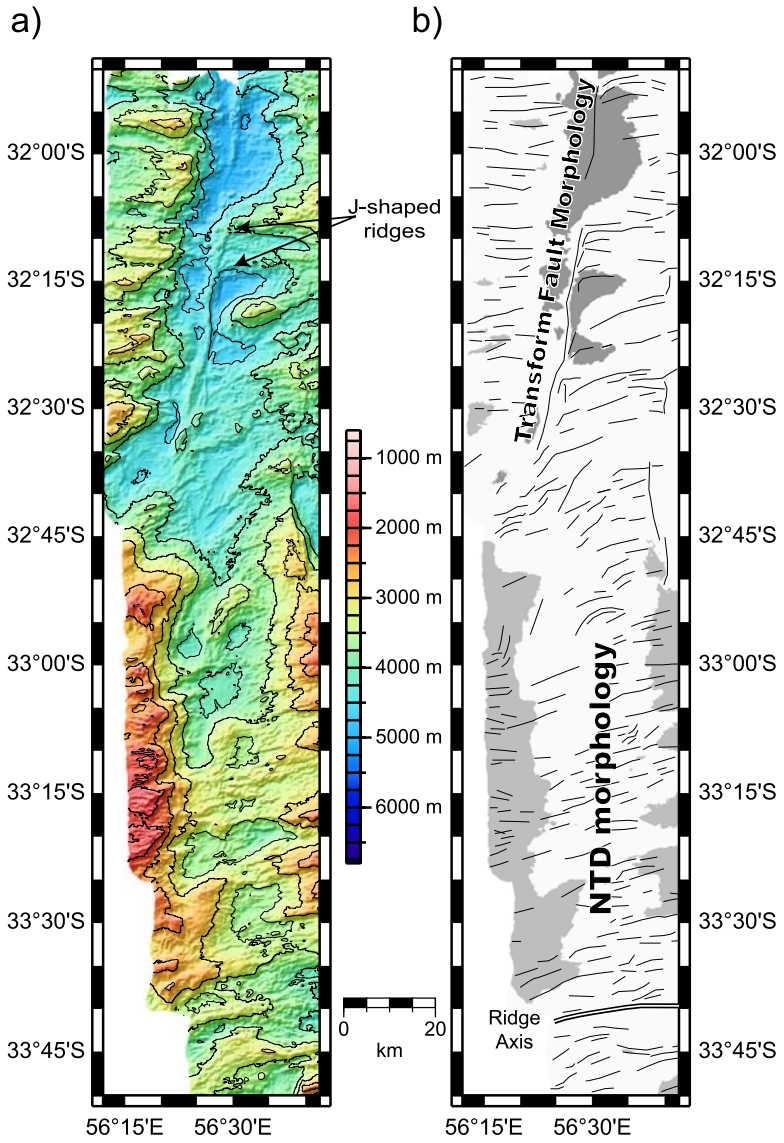

Figure 11. Morphology of the off-axis trace of the 56°30′E nontransform discontinuity: (a) multibeam bathymetry and (b) structural lineations and interpretation. Bathymetry above 3000 m is shaded light gray, while bathymetry lower than 4500 m is shaded dark gray.

northern flank of GA-5 between C6n and C9r (19.2–28.1 Ma) suggest a relatively constant half-spreading rate to the north since C9r and are consistent with symmetric spreading. For this reason and in the absence of additional constraints, our reconstructions of paleoplate boundary geometry (Figure 10) assume symmetric spreading for segments GA-3 and GA-5.

7.2. 56°30′E Nontransform Discontinuity

[47] Spreading rates determined for segment GA-5 suggest approximately symmetric spreading rates since at least 19.2 Ma (Figure 8a). In contrast, spreading in segment GA-6 was highly asymmetric (31%). Together these data imply that spreading-parallel offset of the intervening 56°30′E nontransform discontinuity was greater in the past. A plot of spreading-parallel offset against time (Figure 9a) shows that from 28.1–19.2 Ma (C9r–C6n), the offset was ~45-km-long. Since 19.2 Ma (C6n) the spreading-parallel offset decreased at an average rate of ~1.8 km/Myr (Figure 9a) to reach its current offset of 11 km. The decrease in offset inferred from magnetic data is consistent with a change in the seafloor morphology of the 56°30′E fracture zone observed on multibeam bathymetry data (Figure 11). South of 32°45′S the fracture zone trends ~000°N and is marked by a broad, low amplitude depression with abyssal hills continuous

across it. This morphology is similar to the off-axis expression of nontransform discontinuities at the MAR [*Tucholke et al.*, 1997] and other nontransform discontinuities on the SWIR (e.g., at 57°45′E, Figure 2). North of 32°45′S the fracture zone forms a pronounced depression that trends 010°N. No abyssal hills cross this depression and J-shaped ridges curve into a ridge that runs parallel to the depression (Figure 11). This morphology is similar to that observed at the Atlantis II and Novara Fracture Zones (Figure 2) and suggests that the 56°30′E nontransform discontinuity was previously a transform fault. The change in orientation and morphology of the fracture zone coincide with the 10° counterclockwise rotation in plate-spreading direction during C6n (~19 Ma). The change in fracture zone morphology is sudden and suggests a rapid change from a transform fault to a nontransform discontinuity that may have been facilitated by the observed change in plate-spreading direction. Unfortunately, there are no magnetic data available from 11–19 Ma in segment GA-5 so we are unable to determine whether this sudden change in morphology was accompanied by a rapid change in spreading-parallel offset. However, the available data (Figure 9a) show that this ridge offset has gradually shortened from 30 km to 11 km since 11 Ma; an observation consistent with a steady decrease in ridge offset from >45 km to 11 km since 19 Ma.

7.3. Atlantis II Transform Fault

[48] The direction of asymmetric spreading changes across the Atlantis II transform fault from fast-to-the-north in segment GA-6, to fast-to-the-south in segment AN-1. This requires that the transform fault has lengthened at an average rate of 3.6 km/Myr since 25.7 Ma (Figure 9b). This rate is 0.6 km/Myr faster than that inferred by *Hosford et al.* [2003], which reflects our observation of greater spreading asymmetry in segment GA-6 than was previously assumed. The result of this growth is that the length of the transform fault has increased by >90 km (83%) since 25.7 Ma (Figure 9b). Why the transform fault has grown is unclear, but may, in part, be related to shortening of the nearby 56°30′E paleotransform fault. However, net growth of the Atlantis II transform fault greatly exceeds shortening of the 56°30′E nontransform discontinuity.

[49] If it is assumed that the current rate at which the Atlantis II transform fault is growing has been constant since the inception of the fault, the Atlantis II transform fault would have zero offset ~55 Ma, approximately the time at which the SWIR formed in this location. This observation suggests that the Atlantis II transform fault did not form during triple junction migration, but rather developed since that time.

7.4. 57°40′E Nontransform Discontinuity

[50] The nontransform discontinuity at 57°40′E has had a relatively complicated history [*Hosford and Lin*, 2002; *Hosford et al.*, 2003] and our results are consistent with those that have been presented previously. From 24.3–12.7 Ma (C7n–C5Ar) this nontransform discontinuity had an average offset of 22 ± 2 km. From 12.7–10.4 Ma (C5Ar to C5n), the nontransform discontinuity abruptly shortened (Figure 9c), and this reduction may be related to detachment faulting and the formation of Atlantis Bank [*Baines et al.*, 2005]. From 10.4–3.9 Ma (C5n–C2Ar) the offset was almost constant at 8 ± 2 km; however, between 3.9–3.0 Ma (C2Ar and C2An) the offset increased to ~17 km, the offset seen today [*Hosford et al.*, 2003].

[51] Similar changes in offset across nontransform discontinuities have been observed at the MAR [e.g., *Tucholke et al.*, 1997] where nontransform discontinuities even change their sense of offset while remaining in the same location along the ridge-axis. This implies that nontransform discontinuities are dynamic features that reflect poorly understood processes occurring in the lithosphere or asthenospheric mantle [e.g., *Hosford and Lin*, 2002; *Phipps Morgan and Parmentier*, 1995; *Schouten et al.*, 1985].

7.5. Novara Transform Fault

[52] The two-phase spreading history of segment NM-1 (Figure 8e) dominates the evolution of the Novara transform fault (Figure 9d). Before ~15 Ma the half-spreading rate to the south was ~10.6 km/Myr, whereas since ~15 Ma the half-spreading rate has been ~6.8 km/Ma. This constraint, together with the relatively complicated history of asymmetric spreading in segment AN-2, leads to the Novara transform fault having approximately the same length today (45 km) as it had ~25.7 Ma (50 ± 4 km). However, in the intervening time, the length of the Novara transform fault has not been constant. Fast-to-the-south spreading in NM-1 relative to AN-2 from 26–15 Ma resulted in growth of the Novara transform fault to over 60 km at 15 Ma. But since 10 Ma, fast-to-the-south spreading in AN-2 relative to NM-1 has reduced the offset of the Novara transform fault to its present length of 45 km.

7.6. Between Segment NM-1 and Segment MR-2

[53] Although there are several intervening spreading segments between segment NM-1 and segment MR-2, symmetric spreading in segment NM-1 contrasting with fast-to-the-south spreading in segment MR-2 requires that segment MR-2 has migrated ~15 km north relative to segment NM-1 over the past 15 Myr. Unfortunately without further data we cannot fully constrain how ridge-migration was accommodated by the intervening Melville transform fault, the nontransform discontinuity at 60°08′E and/or the two oblique spreading segments (NM-2ob and MR-1ob). However, by analogy to the growth of the Atlantis II transform fault, we suggest that ridge-migration may have been primarily accommodated by growth of the Melville transform fault.

7.7. Between Segment MR-2 and 64°E

[54] East of segment MR-2, the magmatic spreading segment at 64°E (MR-6) has been spreading symmetrically since ~11 Ma (the end of C5n) [*Cannat et al.*, 2003]. When compared to the asymmetric spreading rates within segment MR-2 this suggests that total spreading-parallel offset between these two magmatic spreading segments may have reduced slightly (~10 km). Although relatively small, such a change in offset must have been accommodated by rotation of one or both of the intervening oblique spreading segments.

7.8. Regional Synthesis

[55] From a regional perspective, the total spreading-parallel offset of all the transform faults, nontransform discontinuities and oblique spreading segments from 54°E–58°45′E along the SWIR has increased by more than 45 km (14%) since 26 Ma. This increase was accommodated primarily by growth of the Atlantis II transform fault. The rotation in plate spreading direction during C6n (~19 Ma) might be expected to reduce the total length of spreading-parallel offsets from 55°E to 58°45′E by 10% not increase it by 14% (Figure 3) suggesting another driving force for the changes in plate-boundary geometry.

8. Discussion

8.1. Asymmetric Spreading at the SWIR

[56] We present evidence for major changes in the geometry of a >400-km-wide section of the eastern SWIR between 54°30′E and 58°45′E since 26 Ma (Figure 10). Variations in the magnitude and/or direction of asymmetric spreading between adjacent spreading segments accommodated these changes, which include growth of the Atlantis II Transform fault from ~110 km to 199 km (Figure 9b), and shortening of a transform fault at 56°30′E by 34 km to form an 11 km offset nontransform discontinuity (Figure 9a). While asymmetric spreading produced local changes in the shape of the plate-boundary, regionally the eastern SWIR is located mid-way between the triple-junction traces to the north and south (Figure 1) implying that, when averaged over its length, the eastern SWIR has been spreading symmetrically since it formed.

[57] To explain the changes in plate boundary geometry we need to understand why individual segments of the SWIR have been spreading asymmetrically. Several mechanisms have been suggested to account for asymmetric spreading at mid-ocean ridges but none are consistent with our observations. *Hosford et al.* [2003] inferred that the SWIR between the Atlantis II transform fault and Melville transform fault has been undergoing uniform fast-to-the-south asymmetric spreading and that this asymmetric spreading is driven by dynamic forces that operate on scales less than 10^3 km. However, our observations of symmetric spreading in segment NM-1 since 15.6 Ma and the opposite sense of asymmetric spreading in segment GA-6 compared to segments AN-1 and AN-2 do not support this inference. In other areas of the mid-ocean ridge system, asymmetric spreading has been attributed to thermal perturbations in the mantle associated with nearby hot spots [*Hayes*, 1976; *Small*, 1995; *Müller et al.*, 1998]; however, no hot spots or thermal anomalies have been identified close to our study area, so this mechanism cannot explain our observations. Migration of mid-ocean ridges over a stationary mantle [*Stein et al.*, 1977] has also been proposed to explain asymmetric spreading rates, but in the hot spot reference frame the eastern SWIR has been migrating to the west-northwest [*Gripp and Gordon*, 2002] which is inconsistent with asymmetric north-south directed spreading on the SWIR, and such a mechanism is inconsistent with the local variations in the sense of asymmetric spreading we have observed. Lastly, *Fujita and Sleep* [1978] suggested that asymmetric spreading might be observed locally at the ends of individual magmatic segments due to the distribution of stresses associated with transform faults. However, our results are also inconsistent with this model, as they show that

entire spreading segments have been spreading asymmetrically. Clearly, none of the mechanisms described above can account for the observed pattern of asymmetric spreading.

8.2. Growth of the Atlantis II Transform Fault and the Causes of Plate Boundary Reorganization

[58] Given that the causes of asymmetric spreading at the SWIR are somewhat ambiguous, we proceed with the assumption that the changes in plate-boundary geometry are not only the result of but also the reason for asymmetric spreading. So in the following discussion, we review and evaluate the possible explanations fro the observed changes in plate-boundary geometry at the SWIR. Major changes in the geometry of mid-ocean ridges have previously been linked to changes in the direction and/or rate of plate-motion [e.g., *Atwater*, 1989; *Hey*, 1977; *Phipps Morgan and Parmentier*, 1995] where the changes in the geometry of plate-boundaries were accomplished by short-lived periods of asymmetric spreading and/or discrete ridge jumps. Here we discuss how changes in plate-motion direction and rate may have affected the plate boundary at the SWIR.

[59] The SWIR from 54°30′E to 58°45′E formed approximately 53 Ma by northeastward migration of the Rodriguez Triple Junction. The wake-like triple junction traces formed during this migration are clear in the satellite-derived bathymetry (Figure 1). These traces show no major changes in orientation (or offset) that can be correlated with the formation of large offset transform faults during triple-junction migration. In fact, the only significant "jog" in the triple junction trace coincides with the fracture zone of the 57°45′E nontransform discontinuity, rather than the Atlantis II transform fault. The poorly defined NNW-SSE trending ends of fracture zones suggest that spreading was initially directed in a NNW-SSE direction. Hence the total spreading-parallel offset of the 1000-km-long 045° trending SWIR from 52° to 61°E was probably <200 km (Figure 12) and the ridge-axis may have more closely resembled that observed west of the Gallieni Transform fault, east of the Melville Transform fault (Figure 1) [*Cannat et al.*, 2003] or from 9°E–16°E [*Dick et al.*, 2003] where there are no large transform faults.

[60] At 40 Ma, there was a ~35° clockwise rotation in plate-spreading direction, as seen by the change in fracture zone trends from ~335° to 010° (Figure 1). After the change in spreading direction the total spreading-parallel offset would have increased from <200 km to ~800 km between the Gallieni and Melville transform faults (Figure 3). We suggest that the abrupt change in bathymetric morphology to crenulated terrain after ~40 Ma reflects formation of the current pattern of along-axis segmentation comprising ten magmatic spreading segments separated by nine spreading parallel ridge-offsets, which may have been transform faults, nontransform discontinuities or oblique amagmatic spreading segments. We infer that this response was rapid given the abrupt change in off-axis morphology and orientation of fracture zones (Figure 1b). The spreading-parallel displacement of the SWIR across each of these nine offsets may initially have been relatively uniform (~70 km offset each), a prediction consistent with our reconstruction of ridge segmentation at 26 Ma (Figure 10 and Figure 12).

[61] Subsequently, there was a 10° counterclockwise rotation in spreading direction during C6n (~19 Ma) [*Dick et al.*, 1991; *Hosford et al.*, 2003] shown by clear changes in the orientation of fracture zones in both the multibeam bathymetry data (Figure 2) and regional satellite bathymetry data (Figure 1). This second change in plate-spreading direction might be expected to decrease the length of any spreading-parallel offset by ~10% (Figure 3), a view consistent with the change in off-axis morphology of the 56°30′E nontransform discontinuity from that characteristic of a larger offset transform fault before C6n (~19 Ma) to that of a smaller offset nontransform discontinuity afterward. However, the inferred decrease in total spreading-parallel offset is not consistent with continued growth of the Atlantis II transform fault and the increase in total offset between 54°45′E to 58°45′E since C6n (~19 Ma) (Figure 9b).

[62] The apparently rapid reaction of the SWIR to the rotations in plate-spreading direction at ~40 Ma and ~19 Ma is not consistent with long-term growth of the Atlantis II transform fault (Figure 9b). We suggest that growth of the Atlantis II transform fault reflects the evolution of the SWIR to form suborthogonal first-order spreading segments (Figure 12). If true, we may be observing the process by which first-order segmentation developed at other mid-ocean ridges. Commonly first-order spreading segments are suborthogonal to the plate-spreading direction, so the highly oblique trend of the two 450-km-long first-order segments between the Gallieni and Melville transform faults

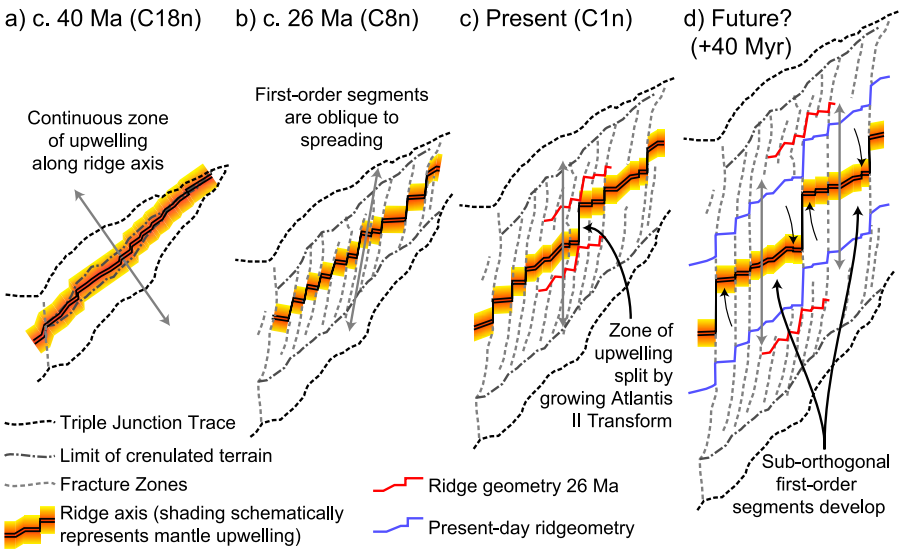

Figure 12. Evolution of the SWIR between the Gallieni and Melville transform faults. (a) Before 40 Ma, the ridge was approximately perpendicular to spreading direction, so spreading-parallel offsets were small. Although they are not linear, the triple junction traces show no evidence for large transform faults. Mantle upwelling and melting may have been relatively continuous along-axis. Shading along the ridge-axis schematically represents a zone of mantle upwelling and melting beneath the ridge-axis; it approximates the width of upwelling for isoviscous 2-D corner flow at 60 km depth. (b) Following a clockwise rotation of plate spreading direction circa 40 Ma, the SWIR rapidly developed evenly spaced ridge offsets, and crenulated bathymetry began to form. Here we show how the SWIR may have looked ~26 Ma. The red line shows the plate boundary geometry reconstructed in Figure 10f. (c) The ridge geometry continued to evolve to produce the present geometry, mainly by growth of the Atlantis II transform fault and the reduction in length of offsets either side of it. The Atlantis II transform fault may now separate zones of mantle upwelling. (d) The possible future geometry, as the Gallieni, Atlantis II, and Melville Transform Faults grow at the expense of intervening offsets to create two suborthogonal first-order segments.

is atypical of mid-ocean ridges. While both of these first-order segments remain relatively oblique to spreading, we note that growth of the Atlantis II transform fault has substantially reduced this obliquity by rotating the first order segments from an orientation of ~045° to ~060° over the last 40 Ma (Figure 12).

[63] Presumably the suborthogonal first-order segmentation of mid-ocean ridges represents a stable geometry for seafloor spreading [*Vogt et al.*, 1969; *Van Andel*, 1971; *Lachenbruch and Thompson*, 1972] but the reasons why such a geometry is preferred are unclear. Two possible explanations are that the evolution of the plate-boundary is controlled by mantle-flow and melt generation within the asthenospheric mantle or it is controlled by shallow lithospheric deformation.

[64] Commonly first-order segmentation has been linked to mantle flow processes, where each segment represents a broad zone or cell of upwelling mantle [e.g., *Whitehead et al.*, 1984; *Macdonald et al.*, 1988]. Higher-order segmentation may represent more shallow focusing of mantle upwelling and melting on a shorter wavelength [e.g., *Magde and Sparks*, 1997; *Choblet and Parmentier*, 2001; *Jousselin et al.*, 1998]. Growth of the Atlantis II transform fault over the past 26 Ma has the effect of decreasing the obliquity of two upwelling cells, one between the Gallieni and Atlantis II transform faults and the other between the Atlantis II and Melville transform faults (Figure 12). If growth of the Atlantis II transform fault is a response to underlying asthenospheric upwelling, then it implies that the preferred geometry for a first-order upwelling cell is perpendicular to spreading and that a spreading ridge will evolve so that first-order segments are approximately orthogonal to spreading. The development of orthogonal spreading segments minimizes the along-axis length of upwelling (Figure 12) leading to more focused and increased mantle upwelling rates [e.g., *Dick et al.*, 2003; *Montesi et al.*, 2005]. At slow- and ultra-slow-spreading rates the temperature beneath the ridge-axis is highly dependent on the rate of mantle upwelling, so a small increase in upwelling rate

beneath an ultraslow-spreading ridge will produce a significant increase in temperature at a given depth beneath the ridge axis. Given the temperature dependence of mantle rheology [e.g., *Hirth and Kohlstedt*, 2003], elevated temperatures beneath the ridge axis will thin the lithosphere, and weaken the ridge-axis, thus reducing the total viscous dissipation of energy associated with mantle flow. So rotation of first-order spreading segments to become more orthogonal to spreading direction may be driven by an attempt to maximize mantle upwelling rates and increase temperatures beneath the ridge-axis. This would weaken the ridge-axis allowing seafloor spreading to occur more easily.

[65] At mid-ocean ridges, mantle upwelling is a passive response to separation of the overlying lithospheric plates, where this separation is driven by far-field forces [e.g., *Lachenbruch*, 1976; *MELT Seismic Team*, 1998]. Therefore the process by which the ridge geometry adapted at the SWIR must be dependent not only on the properties of mantle upwelling but also on the overlying structure of the lithosphere. This interaction is especially important at ultraslow-spreading ridges where lithosphere is cool, strong and thick, even at the ridge axis [e.g., *Rommevaux-Jestin et al.*, 1997]. So an alternative hypothesis is that the evolution of the plate-boundary is controlled by shallow deformation in the lithosphere and particularly deformation along the spreading-parallel offsets of the SWIR. For this hypothesis to hold it must be easier to deform one large transform fault and several smaller ridge offsets than the same number of moderately sized ridge offsets. This inference appears to be at odds with recent observations of the seismicity of oceanic transform faults that suggest that the cumulative seismic moment of a transform fault is proportional to (transform fault length)$^{1.5}$ [*Boettcher and Jordan*, 2004]. If we use cumulative seismic moment as a proxy for the work-done on a transform fault, then this relationship implies that it is easiest to deform multiple transform faults when they are all the same length. Thus growth of the Atlantis II transform fault and the development of suborthogonal first-order segmentation may not be a response to shallow deformation along spreading-parallel ridge offsets but may be primarily controlled by asthenospheric mantle flow. Another potential consequence of thick lithosphere at the SWIR is that it may have acted to slow the ridge's evolution. Intuitively it is harder for a ridge to "jump" in thick strong lithosphere at ultraslow-spreading ridges than in thin, weak lithosphere at fast spreading ridges where segmentation could evolve rapidly [e.g., *Atwater*, 1989]. Thus thick axial lithosphere may explain the gradual evolution and prolonged asymmetric spreading observed at the SWIR.

[66] We suggest that the SWIR will continue to evolve with the Atlantis II, Gallieni and Melville transform faults continuing to grow while intervening spreading-parallel offsets shrink, so that SWIR between these transform faults becomes more orthogonal to spreading (Figure 12d). Thus we propose that the change in plate-spreading direction at 40 Ma had two major effects: in the short term it led to rapid changes in the morphology of the SWIR and initiated the current pattern of second-order segmentation, but it also increased the overall obliquity of the SWIR and formed oblique first-order segments. These oblique first-order segments do not represent a stable configuration for plate-spreading, so the SWIR has been slowly evolving to attain more stable suborthogonal first-order segmentation. This evolution is facilitated by the observed variation in spreading rate asymmetry along the ridge axis.

8.3. Stability of Oblique Spreading Segments

[67] Segment GA-4ob has maintained its current geometry since at least ~11 Ma and its trend is similar to the overall 045°N trend of the ridge axis. A satellite gravity low associated with this segment can be traced off-axis to at least 40 Ma (Figure 1) led *Dick et al.* [2003] to suggest that this oblique spreading segment has been stable with its current geometry since the SWIR formed. The observed stability since ~11 Ma and the inferred stability since 40 Ma is in marked contrast to nearby transform faults and nontransform discontinuities that have undergone dramatic changes in spreading-parallel offset.

[68] *Dick et al.* [2003] inferred that oblique spreading segments only form when the full-spreading rate is <20 km/Myr; however, before 19.2 Ma (C6n) the full-spreading rate of the SWIR was >20 km/Myr (Table 1), while before C6Cn the full-spreading rate may have been >30 km/Myr [*Cannat et al.*, 2006]. So if the formation of amagmatic segments is only dependent on the full-spreading rate, segment GA-4ob would not be an oblique spreading segment before 19.2 Ma, but may instead have taken the form of a nontransform discontinuity or transform fault. However, where oblique amagmatic segments are currently observed east of the Melville transform fault,

bathymetry data that extends beyond 19.2 Ma show no evidence for a change in the style of segmentation associated with these changes in full-spreading rate [*Cannat et al.*, 2006]. Therefore spreading rate is unlikely to be the only control on the formation of oblique amagmatic spreading segments; mantle potential temperature and chemistry may play an important role in the observed mode of spreading [*Dick et al.*, 2003]. For example where a mid-ocean ridge is extending itself by propagation, as at Hess Deep in the Pacific, the lithosphere may be thicker and stronger than usual, with a low magma budget, resulting in the formation of oblique rifts at spreading rates where they normally would not form. Further multibeam bathymetric and magnetic data that extend >19.2 Ma off-axis from 54°E to 57°E along the SWIR are needed to determine the longevity and spreading rate dependence of the oblique amagmatic spreading for segment GA-4ob.

[69] Despite uncertainty about the character of segment GA-4ob before 19.2 Ma, segment GA-4ob has been stable since 11 Ma [*Mendel et al.*, 2003], which contrasts with the observed changes in the offset of nearby nontransform discontinuities and transform faults. Amagmatic spreading segments may be inherently more stable than nontransform discontinuities and transform faults. *Dick et al.* [2003] suggest that low magma budgets play a major role in stabilizing oblique amagmatic spreading segments. Where there is a high magma budget, diking dramatically weakens the lithosphere and occurs orthogonal to the least principal stress direction, which is generally parallel to the spreading direction. This causes magmatic segments to form suborthogonal to spreading. Along amagmatic spreading segments where diking does not occur, the lithosphere is thicker and a zone of lithospheric necking may persist with the same geometry for a considerable time, the result being that, once established, the geometry of an amagmatic spreading segment will be relatively difficult to change.

[70] Alternatively the stability of segment GA-4ob may be reconciled using the model discussed above in which oblique first-order segments are rotating to become more orthogonal to spreading. Segment GA-4ob is located at the center of a rotating first-order segment where the driving forces for and the distance of rotation are less than at the edges of the first-order segment. So we suggest that the recent stability of segment GA-4ob since 11 Ma is due to its position at the center of a rotating first-order segment.

9. Conclusions

[71] We have used magnetic and bathymetric data recorded over >130,000 km^2 to deduce the spreading history of the SWIR from 54°E–59°E since 26 Ma. Although on a regional scale (>450 km), plate-motion has been symmetric for the eastern SWIR, individual spreading segments have been spreading asymmetrically. Variation in the direction and magnitude of spreading asymmetry between adjacent spreading segments produced changes in the spreading-parallel offsets of both transform faults and nontransform discontinuities:

[72] 1. A 45-km-long transform fault at 56°30′E has shortened and evolved to become the 11-km-offset nontransform discontinuity.

[73] 2. The Atlantis II Transform fault has grown by >90 km to reach a current length of 199 km.

[74] 3. The offset across the nontransform discontinuity at 57°40′E, abruptly decreased from 12.7–10.4 Ma (C5Ar to C5n). More recently (3.9–3.0 Ma), the offset increased to ~17 km, the offset seen today. We note that reduction in offset 12.7–10.4 Ma coincides with detachment faulting and the formation of Atlantis Bank.

[75] 4. The Novara transform fault grew from 45 km 26 Ma to 60 km at 15 Ma, but its length has since reduced to 45 km.

[76] These observations from nontransform discontinuities and transform faults contrast with the recent (<11 Ma) stability of the oblique amagmatic spreading segment GA-4ob to the west. To account for the above observations, we suggest the following model for the evolution of the SWIR from 52°E–61°45′E (Figure 12):

[77] 1. This section of the SWIR formed from 40–64 Ma by NE migration of the Rodriguez Triple Junction between oceanic lithosphere created at the CIR and SEIR. During this period the SWIR was approximately orthogonal to the NNW-SSE directed spreading and irregular off-axis bathymetry formed. These observations suggest that there were only minor spreading parallel offsets of the ridge at this time and no major transform faults existed.

[78] 2. At ~40 Ma, a ~35° clockwise rotation in plate spreading direction increased the overall obliquity of the SWIR to plate-spreading direction,

led to rapid changes in the morphology of the SWIR and initiated the current pattern of second-order segmentation producing crenulated off-axis terrane (Figure 1). The offset of the SWIR across each of the nine spreading-parallel ridge-offsets is likely to have been similar such that oblique first-order spreading segments were created.

[79] 3. After 40 Ma, growth of the Atlantis II transform fault at the expense of adjacent spreading-parallel ridge-offsets, led to rotation of the adjacent first-order spreading segments to become more orthogonal to spreading. The recent (<11 Ma) stability of segment GA-4ob may reflect either weaker driving forces for changes in spreading geometry at the center of a rotating first-order spreading segment or the inherent stability of oblique spreading segments compared to nontransform discontinuities and transform faults.

[80] 4. We predict that the other large offset transform faults that bound the 450-km-wide first-order segments (the Melville and Gallieni transform faults) have also grown to further reduce the obliquity of the first-order spreading segments, while the intervening small offset transform faults and nontransform discontinuities have reduced their offset. This inference is consistent with the fast-to-the-south asymmetric spreading observed in segment MR-2.

[81] Segmentation at the eastern SWIR is unrelated to continental break-up but the pattern of segmentation that is developing is similar to that observed at other mid-ocean ridges that formed by continental rupture. Therefore suborthogonal first-order spreading segments at other mid-oceanic ridges may have evolved in a similar manner to that progressing at the eastern SWIR. Suborthogonal first-order spreading segments likely represent a stable configuration for plate-spreading because they maximize upwelling rates in the asthenospheric mantle and result in a hotter and weaker ridge-axis that can more easily accommodate seafloor spreading.

Acknowledgments

[82] We thank the captain and crew of the R/V *Yokosuka* and the *Shinkai 6500* operations team during cruise YK01-14. This manuscript benefited from constructive reviews by Maurice Tivey and Doug Wilson. Funding for this work came from a JOI-Schlanger Fellowship to Baines and NSF grant 0352054 to Cheadle and John.

References

Allerton, S., and M. A. Tivey (2001), Magnetic polarity structure of the lower oceanic crust, *Geophys. Res. Lett.*, *28*, 423–426.

Arai, S., H. J. B. Dick, and Shipboard Scientific Party (2001), Mode 2000 leg 6 cruise report, Jpn. Mar. Sci. and Technol. Agency, Yokosuka.

Arkani-Hamed, J. (1988), Remanent magnetization of the oceanic upper mantle, *Geophys. Res. Lett.*, *15*, 48–51.

Atwater, T. (1989), Plate tectonic history of the northeast Pacific and western North America, in *The Eastern Pacific Ocean and Hawaii*, edited by E. L. Winterer, D. M. Hussong, and R. W. Decker, pp. 21–72, Geol. Soc. Am., Denver, Colo.

Baines, A. G., M. J. Cheadle, H. J. B. Dick, A. Hosford Scheirer, B. E. John, N. J. Kusznir, and T. Matsumoto (2003), A mechanism for generating the anomalous uplift of oceanic core-complexes: Atlantis Bank, SW Indian Ridge, *Geology*, *31*(12), 1105–1108.

Baines, A. G., M. J. Cheadle, B. E. John, and J. J. Schwartz (2005), Time-averaged rate of detachment faulting at Atlantis Bank, Southwest Indian Ridge: Evidence for highly asymmetric spreading rates during the formation of oceanic core-complexes, *Eos Trans. AGU*, *86*(52), Fall Meet. Suppl., Abstract T32A-03.

Batiza, R. (1996), Magmatic segmentation of mid-ocean ridges: A review, in *Tectonic, Magmatic, Hydrothermal and Biological Segmentation of Mid-Ocean Ridges*, edited by C. J. MacLeod, P. A. Tyler, and C. L. Walker, *Spec. Publ. Geol. Soc. London*, *118*, 103–130.

Bina, M. M., and B. Henry (1990), Magnetic properties, opaque mineralogy and magnetic anisotropies of serpentinized peridotites from ODP Hole 670A near the Mid-Atlantic Ridge, *Phys. Earth Planet. Inter.*, *65*, 88–103.

Boettcher, M. S., and T. H. Jordan (2004), Earthquake scaling relations for mid-ocean ridge transform faults, *J. Geophys. Res.*, *109*, B12302, doi:10.1029/2004JB003110.

Cande, S. C., and D. V. Kent (1995), Revised calibration of the geomagnetic polarity timescale for the Late Cretaceous and Cenozoic, *J. Geophys. Res.*, *100*, 6093–6095.

Cannat, M., C. Rommevaux-Jestin, D. Sauter, C. Deplus, and V. Mendel (1999), Formation of the axial relief at the very slow spreading Southwest Indian Ridge (49° to 57°E), *J. Geophys. Res.*, *104*, 22,825–22,843.

Cannat, M., C. Rommevaux-Jestin, and H. Fujimoto (2003), Melt supply variations to a magma-poor ultra-slow spreading ridge (Southwest Indian Ridge 61°–69°E), *Geochem. Geophys. Geosyst.*, *4*(8), 9104, doi:10.1029/2002GC000480.

Cannat, M., D. Sauter, V. Mendel, E. Ruellan, K. Okino, J. Escartin, V. Combier, and M. Baala (2006), Modes of seafloor generation at a melt-poor ultraslow-spreading ridge, *Geology*, *34*, 605–608.

Carbotte, S., S. M. Welch, and K. C. Macdonald (1991), Spreading rates, rift propagation, and fracture zone offset histories during the past 5 my on the Mid-Atlantic Ridge: 25°–27°30′S and 31°–34°30′S, *Mar. Geophys. Res.*, *13*, 51–80.

Caress, D. W., and D. N. Chayes (1996), Improved processing of hydrosweep DS multibeam data on the R/V *Maurice Ewing*, *Mar. Geophys. Res.*, *18*, 631–650.

Choblet, G., and E. M. Parmentier (2001), Mantle upwelling and melting beneath slow spreading centers: Effects of variable rheology and melt productivity, *Earth Planet. Sci. Lett.*, *184*, 589–604.

Chu, D., and R. G. Gordon (1999), Evidence for motion between Nubia and Somalia along the Southwest Indian Ridge, *Nature*, *398*, 64–67.

Cochran, J. R., G. J. Kurras, M. H. Edwards, and B. J. Coakley (2003), The Gakkel Ridge: Bathymetry, gravity anomalies, and crustal accretion at extremely slow spreading rates, *J. Geophys. Res.*, *108*(B2), 2116, doi:10.1029/2002JB001830.

DeMets, C., R. G. Gordon, D. F. Argus, and S. Stein (1994), Effect of recent revisions to the geomagnetic reversal time scale on estimates of current plate motions, *Geophys. Res. Lett.*, *21*, 2191–2194.

Dick, H. J. B. (1989), Abyssal peridotites, very slow spreading ridges and ocean ridge magmatism, in *Magmatism in the Ocean Basins*, edited by A. D. Saunders and M. J. Norry, *Geol. Soc. Spec. Publ.*, *42*, 71–105.

Dick, H. J. B., H. Schouten, P. S. Meyer, D. G. Gallo, H. Bergh, R. Tyce, P. Patriat, K. T. M. Johnson, J. Snow, and A. Fisher (1991), Tectonic evolution of the Atlantis II Fracture Zone, *Proc. Ocean Drill. Program Sci. Results*, *118*, 359–398.

Dick, H. J. B., J. Lin, and H. Schouten (2003), An ultraslow-spreading class of ocean ridge, *Nature*, *426*, 405–412.

Dyment, J. (1993), Evolution of the Indian Ocean triple junction between 65 and 49 Ma (anomalies 28 to 21), *J. Geophys. Res.*, *98*, 13,863–13,877.

Dyment, J., J. Arkani-Hamed, and A. Ghods (1997), Contribution of serpentinized ultramafics to marine magnetic anomalies at slow and intermediate spreading centres: Insights from the shape of the anomalies, *Geophys. J. Int.*, *129*, 691–701.

Dziak, R. P., C. G. Fox, R. W. Embley, J. L. Nabelek, J. Braunmiller, and R. A. Koski (2000), Recent tectonics of the Blanco Ridge, eastern Blanco transform fault zone, *Mar. Geophys. Res.*, *21*, 423–450.

Fox, P. J., and N. Opdyke (1973), Geology of the oceanic crust: Magnetic properties of oceanic rocks, *J. Geophys. Res.*, *78*, 5139–5154.

Fujita, K., and N. H. Sleep (1978), Membrane stresses near mid-ocean ridge-transform intersections, *Tectonophysics*, *50*, 207–221.

Grindlay, N. R., J. A. Madsen, C. Rommevaux-Jestin, and J. G. Sclater (1998), A different pattern of ridge segmentation and mantle Bouguer gravity anomalies along the ultra-slow spreading Southwest Indian Ridge (15°30′E to 25°E), *Earth Planet. Sci. Lett.*, *161*, 243–253.

Gripp, A. E., and R. G. Gordon (2002), Young tracks of hotspots and current plate velocities, *Geophys. J. Int.*, *150*, 321–361.

Hayes, D. E. (1976), Nature and implications of asymmetric sea-floor spreading; "different rates for different plates", *Geol. Soc. Am. Bull.*, *87*, 994–1002.

Hayes, D. E., and K. A. Kane (1994), Long-lived mid-ocean ridge segmentation of the Pacific-Antarctic Ridge and the Southeast Indian Ridge, *J. Geophys. Res.*, *99*, 19,679–19,692.

Hey, R. (1977), Tectonic evolution of the Cocos-Nazca spreading center, *Geol. Soc. Am. Bull.*, *88*, 1404–1420.

Hirth, G., and D. Kohlstedt (2003), Rheology of the upper mantle and the mantle wedge: A view from the experimentalists, in *Inside the Subduction Factory*, *Geophys. Monogr. Ser.*, vol. 138, edited by J. Eiler, pp. 83–105, AGU, Washington, D. C.

Horner-Johnson, B. C., R. G. Gordon, S. M. Cowles, and D. F. Argus (2005), The angular velocity of Nubia relative to Somalia and the location of the Nubia-Somalia-Antarctica triple junction, *Geophys. J. Int.*, *162*, 221–238.

Hosford, A., and J. Lin (2002), Structural evolution from a strike-slip transform fault to a non-transform discontinuity: Examples from 57° to 58°30′E on the SW Indian Ridge and geodynamic implications, *Eos Trans. AGU*, *83*(47), Fall Meet. Suppl., Abstract T52E-04.

Hosford, A., M. A. Tivey, T. Matsumoto, H. J. B. Dick, H. Schouten, and H. Kinoshita (2003), Crustal magnetization and accretion at the Southwest Indian Ridge near the Atlantis II Fracture Zone, 0–25 Ma, *J. Geophys. Res.*, *108*(B3), 2169, doi:10.1029/2001JB000604.

Jousselin, D., A. Nicolas, and F. Boudier (1998), Detailed mapping of a mantle diapir below a paleo-spreading center in the Oman ophiolite, *J. Geophys. Res.*, *103*, 18,153–18,170.

Kane, K. A., and D. E. Hayes (1992), Tectonic corridors in the South Atlantic: Evidence for long-lived mid-ocean ridge segmentation, *J. Geophys. Res.*, *97*, 17,317–17,330.

Kent, D. V., and F. M. Gradstein (1986), A Jurassic to Recent chronology, in *The Western North Atlantic Region*, edited by P. R. Vogt and B. E. Tucholke, pp. 45–50, Geol. Soc. Am., Boulder, Colo.

Kikawa, E., and J. E. Pariso (1991), Magnetic properties of gabbros from Hole 735B, Southwest Indian Ridge, *Proc. Ocean Drill. Program Sci. Results*, *118*, 285–307.

Kinoshita, H., H. J. B. Dick, and Shipboard Scientific Party (2001), Atlantis II Fracture Zone: MODE'98 preliminary report, 221 pp., JAMSTEC Deep Sea Res., Yokosuka, Japan.

Klitgord, K. D., and H. Schouten (1986), Plate kinematics of the central Atlantic, in *The Western North Atlantic Region*, edited by P. R. Vogt and B. E. Tucholke, pp. 351–378, Geol. Soc. Am., Boulder, Colo.

Krammer, K. (1990), Rock magnetic properties and opaque mineralogy of selected samples from Hole 670A, *Proc. Ocean Drill. Program Sci. Results*, *106/109*, 269–273.

Lachenbruch, A. H. (1976), Dynamics of a passive spreading center, *J. Geophys. Res.*, *81*, 1883–1902.

Lachenbruch, A. H., and G. A. Thompson (1972), Oceanic ridges and transform faults: Their intersection angles and resistance to plate motion, *Earth Planet. Sci. Lett.*, *15*, 116–122.

Lemaux, J., R. G. Gordon, and J.-Y. Royer (2002), Location of the Nubia-Somalia boundary along the Southwest Indian Ridge, *Geology*, *30*, 339–342.

Lienert, B. R., and P. J. Wasilewski (1979), A magnetic study of the serpentinization process at Buzzo Mountain, California, *Earth Planet. Sci. Lett.*, *43*, 406–416.

Lourens, L., F. Hilgen, N. J. Shackleton, J. Laskar, and D. Wilson (2004), The Neogene period, in *A Geologic Time Scale 2004*, edited by F. M. Gradstein, J. G. Ogg, and A. G. Smith, pp. 409–440, Cambridge Univ. Press, Cambridge, U. K.

Macdonald, K. C., S. P. Miller, S. P. Huestis, and F. N. Spiess (1980), Three-dimensional modeling of a magnetic reversal boundary from inversion of deep-tow measurements, *J. Geophys. Res.*, *85*, 3670–3680.

Macdonald, K. C., P. J. Fox, L. J. Perram, M. F. Eisen, R. M. Haymon, S. P. Miller, S. M. Carbotte, M. H. Cormier, and A. N. Shor (1988), A new view of the mid-ocean ridge from the behaviour of ridge-axis discontinuities, *Nature*, *335*, 217–225.

Magde, L. S., and D. W. Sparks (1997), Three-dimensional mantle upwelling, melt generation, and melt migration beneath segment slow spreading ridges, *J. Geophys. Res.*, *102*, 20,571–20,583.

Matsumoto, T., H. J. B. Dick, and Shipboard Scientific Party (2002), Investigation of Atlantis Bank and the SW Indian

Ridge from 56°E to 58°E: Preliminary report, 463 pp., JAMSTEC Deep Sea Res., Yokosuka, Japan.
MELT Seismic Team (1998), Imaging the deep seismic structure beneath a mid-ocean ridge: The MELT Experiment, *Science*, *280*, 1215–1218.
Mendel, V., D. Sauter, L. Parson, and J.-R. Vanney (1997), Segmentation and morphotectonic variations along a super slow-spreading center: The Southwest Indian Ridge (57°E–70°E), *Mar. Geophys. Res.*, *19*, 505–533.
Mendel, V., D. Sauter, C. Rommevaux-Jestin, P. Patriat, F. Lefebvre, and L. M. Parson (2003), Magmato-tectonic cyclicity at the ultra-slow spreading Southwest Indian Ridge: Evidence from variations of axial volcanic ridge morphology and abyssal hills pattern, *Geochem. Geophys. Geosyst.*, *4*(5), 9102, doi:10.1029/2002GC000417.
Meyzen, C. M., M. J. Toplis, E. Humler, J. N. Ludden, and C. Mével (2003), A discontinuity in mantle composition beneath the Southwest Indian Ridge, *Nature*, *421*, 731–733.
Michael, P. J., et al. (2003), Magmatic and amagmatic seafloor generation at the ultraslow-spreading Gakkel Ridge, Arctic Ocean, *Nature*, *423*, 956–961.
Montesi, L., M. D. Behn, and J. Barry (2005), On the geodynamics of oblique spreading, *Eos Trans. AGU*, *86*(52), Fall Meet. Suppl., Abstract T32A-06.
Muller, M. R., C. J. Robinson, T. A. Minshull, R. S. White, and M. J. Bickle (1997), Thin crust beneath Ocean Drilling Program Borehole 735B at the Southwest Indian Ridge?, *Earth Planet. Sci. Lett.*, *148*, 93–107.
Muller, M. R., T. A. Minshull, and R. S. White (1999), Segmentation and melt supply at the Southwest Indian Ridge, *Geology*, *27*, 867–870.
Muller, M. R., T. A. Minshull, and R. S. White (2000), Crustal structure of the Southwest Indian Ridge at the Atlantis II Fracture Zone, *J. Geophys. Res.*, *105*, 25,809–25,828.
Müller, R. D., W. R. Roest, J.-Y. Royer, L. M. Gahagan, and J. G. Sclater (1997), Digital isochrons of the world's ocean floor, *J. Geophys. Res.*, *102*, 3211–3214.
Müller, R. D., W. R. Roest, and J.-Y. Royer (1998), Asymmetric sea-floor spreading caused by ridge-plume interactions, *Nature*, *396*, 455–459.
Natland, J. H., and H. J. B. Dick (2002), Stratigraphy and composition of gabbros drilled in Ocean Drilling Program Hole 735B, Southwest Indian Ridge: A synthesis of geochemical data, *Proc. Ocean Drill. Program Sci.*, *179*, doi:10.2973/odp.proc.sr.176.002.2002.
Nazarova, K. A. (1994), Serpentinized peridotites as a possible source for oceanic magnetic anomalies, *Mar. Geophys. Res.*, *16*, 455–462.
Nazarova, K. A., P. J. Wasilewski, and H. J. B. Dick (2000), Magnetic study of serpentinized harzburgites from the Islas Orcadas Fracture Zone, *Mar. Geophys. Res.*, *21*, 475–488.
Ogg, J. G., and A. G. Smith (2004), The geomagnetic polarity time scale, in *A Geological Time Scale 2004*, edited by F. M. Gradstein, J. G. Ogg, and A. G. Smith, pp. 63–86, Cambridge Univ. Press, Cambridge, U. K.
Parker, R. L., and S. P. Huestis (1974), The inversion of magnetic anomalies in the presence of topography, *J. Geophys. Res.*, *79*, 1587–1593.
Patriat, P., and V. Courtillot (1984), On the stability of triple junctions and its relation to episodicity in spreading, *Tectonics*, *3*, 317–332.
Patriat, P., and J. Segoufin (1988), Reconstruction of the central Indian Ocean, *Tectonophysics*, *155*, 211–234.
Patriat, P., et al. (1996), The GALLIENI cruise: A geophysical survey of the South-West Indian Ridge near the Gallieni FZ (37°S, 52°E), *InterRidge News*, *5*, 19–29.
Patriat, P., D. Sauter, M. Munschy, and L. Parson (1997), A survey of the Southwest Indian Ridge axis between Atlantis II Fracture Zone and the Indian Ocean triple junction: Regional setting and large scale segmentation, *Mar. Geophys. Res.*, *19*, 457–480.
Phipps Morgan, J., and E. M. Parmentier (1995), Crenulated seafloor: Evidence for spreading-rate dependent structure of mantle upwelling and melting beneath a mid-oceanic spreading center, *Earth Planet. Sci. Lett.*, *129*, 73–84.
Prince, R. A., and D. W. Forsyth (1984), A simple objective method for minimizing crossover errors in marine gravity data, *Geophysics*, *49*, 1070–1083.
Rommevaux-Jestin, C., C. Deplus, and P. Patriat (1997), Mantle Bouguer anomaly along an ultra slow-spreading ridge: Implications for accretionary processes and comparison with results from central Mid-Atlantic Ridge, *Mar. Geophys. Res.*, *19*, 481–503.
Sandwell, D. T., and W. H. F. Smith (1997), Marine gravity anomaly from Geosat and ERS 1 satellite altimetry, *J. Geophys. Res.*, *102*, 10,039–10,054.
Sauter, D., P. Patriat, C. Rommevaux-Jestin, M. Cannat, A. Briais, and Gallienni Shipboard Party (2001), The Southwest Indian Ridge between 49°15′E and 57°E: Focused accretion and magma redistribution, *Earth Planet. Sci. Lett.*, *192*, 303–317.
Sauter, D., H. Carton, V. Mendel, M. Munschy, C. Rommevaux-Jestin, J.-J. Schott, and H. Whitechurch (2004), Ridge segmentation and the magnetic structure of the Southwest Indian Ridge (at 50°30′E, 55°30′E, and 66°20′E): Implications for magmatic processes at ultraslow-spreading centers, *Geochem. Geophys. Geosyst.*, *5*, Q05K08, doi:10.1029/2003GC000581.
Schouten, H., K. D. Klitgord, and J. A. Whitehead (1985), Segmentation of mid-ocean ridges, *Nature*, *317*, 225–229.
Shipboard Scientific Party (1989), Site 732, *Proc. Ocean Drill. Program Initial Rep.*, *118*, 41–57.
Shive, P. N., B. R. Frost, and A. Peretti (1988), The magnetic properties of metaperidotic rocks as a function of metamorphic grade: Implications for crustal magnetic anomalies, *J. Geophys. Res.*, *93*, 12,187–12,195.
Sinton, J. M., S. M. Smaglik, J. J. Mahoney, and K. C. Macdonald (1991), Magmatic processes at superfast spreading mid-ocean ridges: Glass compositional variations along the East Pacific Rise 13°–23°S, *J. Geophys. Res.*, *96*, 6133–6155.
Small, C. (1995), Observations of ridge-hotspot interactions in the Southern Ocean, *J. Geophys. Res.*, *100*, 17,931–17,946.
Smith, W. H. F., and D. T. Sandwell (1997), Global sea floor topography from satellite altimetry and ship depth soundings, *Science*, *277*, 1956–1962.
Smith, W. H. F., and P. Wessel (1990), Gridding with continuous curvature splines in tension, *Geophysics*, *55*, 293–305.
Stein, S., H. J. Melosh, and J. B. Minster (1977), Ridge migration and asymmetric sea-floor spreading, *Earth Planet. Sci. Lett.*, *36*, 51–62.
Sykes, L. R. (1967), Mechanism of earthquakes and nature of faulting on the mid-oceanic ridges, *J. Geophys. Res.*, *72*, 2131–2153.
Talwani, M., C. C. Windisch, and M. G. Langseth Jr. (1971), Reykjanes Ridge crest: A detailed geophysical study, *J. Geophys. Res.*, *76*, 473–517.
Tucholke, B. E., J. Lin, M. C. Kleinrock, M. A. Tivey, T. B. Reed, J. Goff, and G. E. Jaroslow (1997), Segmentation and crustal structure of the western Mid-Atlantic Ridge flank, 25°25′–27°10′N and 0–29 m. y., *J. Geophys. Res.*, *102*, 10,203–10,223.

Van Andel, T. H. (1971), Fracture zones, *Geophysics*, *1*, 159–166.

Vogt, P. R., O. E. Avery, E. D. Schneider, C. N. Anderson, and D. R. Bracey (1969), Discontinuities in sea-floor spreading, *Tectonophysics*, *8*, 285–317.

Weiland, C. M., K. C. Macdonald, and N. R. Grindlay (1996), Ridge segmentation and the magnetic structure of the southern Mid-Atlantic Ridge 26°S and 31°–35°S: Implications for magmatic processes at slow spreading centers, *J. Geophys. Res.*, *101*, 8055–8073.

Wessel, P., and W. H. F. Smith (1998), New improved version of generic mapping tools released, *Eos Trans. AGU*, *79*, 579.

Whitehead, J. A., Jr., H. J. B. Dick, and H. Schouten (1984), A mechanism for magmatic accretion under spreading centres, *Nature*, *312*, 146–148.

Worm, H.-U. (2001), Magnetic stability of oceanic gabbros from ODP Hole 735B, *Earth Planet. Sci. Lett.*, *193*, 287–302.

York, D. (1966), Least squares fitting of a straight line, *Can. J. Phys.*, *44*, 1079–1086.